

Dark Matter and Gauged Flavor Symmetries

Fady Bishara,^{1,2,*} Admir Greljo,^{3,†} Jernej F. Kamenik,^{4,5,6,‡}

Emmanuel Stamou,^{7,§} and Jure Zupan^{1,¶}

¹*Department of Physics, University of Cincinnati, Cincinnati, Ohio 45221, USA*

²*Theoretical Physics Department, Fermilab, P.O. Box 500, Batavia, IL 60510, USA*

³*Physik-Institut, Universität Zürich, CH-8057 Zürich, Switzerland*

⁴*Jožef Stefan Institute, Jamova 39, 1000 Ljubljana, Slovenia*

⁵*Faculty of Mathematics and Physics, University of*

Ljubljana, Jadranska 19, 1000 Ljubljana, Slovenia

⁶*CERN TH-PH Division, Meyrin, Switzerland*

⁷*Department of Particle Physics and Astrophysics,*

Weizmann Institute of Science, Rehovot 7610001, Israel

(Dated: February 11, 2022)

Abstract

We investigate the phenomenology of flavored dark matter (DM). DM stability is guaranteed by an accidental \mathcal{Z}_3 symmetry, a subgroup of the standard model (SM) flavor group that is not broken by the SM Yukawa interactions. We consider an explicit realization where the quark part of the SM flavor group is fully gauged. If the dominant interactions between DM and visible sector are through flavor gauge bosons, as we show for Dirac fermion flavored DM, then the DM mass is bounded between roughly 0.5 TeV and 5 TeV if the DM multiplet mass is split only radiatively. In general, however, no such relation exists. We demonstrate this using scalar flavored DM where the main interaction with the SM is through the Higgs portal. For both cases we derive constraints from flavor, cosmology, direct and indirect DM detection, and collider searches.

*Electronic address: bisharfy@mail.uc.edu

†Electronic address: admir@physik.uzh.ch

‡Electronic address: jernef.kamenik@cern.ch

§Electronic address: emmanuel.stamou@weizmann.ac.il

¶Electronic address: jure.zupan@cern.ch

Contents

I. Introduction	3
II. Stability of flavored dark matter	4
III. Gauged flavor interactions and dark matter	6
A. Fermionic flavored dark matter	8
B. Scalar flavored dark matter	11
IV. Dark matter and new physics phenomenology	12
A. Scan results	12
B. Thermal relic	14
1. Fermionic dark matter	15
2. Scalar dark matter	18
C. Cosmology	19
D. Direct and indirect dark matter searches	22
E. Searches at the LHC	24
F. Flavor constraints	26
V. Benchmarks	28
VI. Conclusions	34
A. Minimal flavor violation with gauged flavor symmetries	36
B. Thermal relic computation	39
C. Higgs coupling Feynman rules	43
References	43

I. INTRODUCTION

The stability of dark matter (DM) is commonly assumed to be due to an exact discrete symmetry, \mathcal{Z}_n . This can either be imposed by hand or have a dynamical origin. Examples include R -parity in the MSSM [1], and flavor symmetries in the leptonic sector [2–5]. Here, we explore the intriguing possibility raised in Refs. [6, 7] that the stability of DM is due to the \mathcal{Z}_3 center group of the global $\mathcal{G}_F^{\text{SM}} \equiv SU(3)_Q \times SU(3)_U \times SU(3)_D$ quark flavor symmetry. While $\mathcal{G}_F^{\text{SM}}$ is broken by the SM Yukawa interactions, its subgroup \mathcal{Z}_3 remains unbroken in the SM. More generally, it remains exact also in the presence of New Physics (NP), if the flavor breaking is of Minimally Flavor Violating (MFV) type, i.e. only due to the SM Yukawas. The lightest neutral state that is odd under \mathcal{Z}_3 is therefore stable and is a DM candidate. This is the idea behind MFV dark matter [6–8].

Requiring MFV is sufficient, but not necessary. In this paper we formulate a general condition for flavored DM using *flavor triality* (see Eq. (3) below). For example, any spurion in the bifundamental of $\mathcal{G}_F^{\text{SM}}$ leaves the above \mathcal{Z}_3 unbroken. The flavor breaking can thus be quite far from MFV and still have stability of DM guaranteed by the flavor dynamics. To illustrate this point we consider the model of Ref. [9] where the flavor-breaking spurions have the form $Y_{u,d}^{-1}$ and are thus canonically not of the MFV type. In this model the SM quark flavor symmetry $\mathcal{G}_F^{\text{SM}}$ is fully gauged giving rise to flavor-gauge bosons, the Yukawas are promoted to physical scalar fields (flavons) transforming under flavor, and in addition there is a set of chiral fermions that cancel the anomalies in the flavor-gauge sector.

Using this renormalizable model we show below that a thermal relic DM can be in a nontrivial representation of $\mathcal{G}_F^{\text{SM}}$. There are two conflicting constraints on this setup. On the one hand, Flavor Changing Neutral Current (FCNC) constraints impose lower bounds on the masses of states in nontrivial flavor representations. On the other hand, a DM relic density consistent with observations requires large enough DM annihilation cross section so that some of these same particles need to be sufficiently light. Both of these requirements are satisfied for $\mathcal{O}(\text{TeV})$ DM mass. This is low enough that it may be tested by direct and indirect DM detection experiments and searched for at high-energy particle colliders.

While the phenomenology of flavored DM models can be found in Refs. [7, 10–20], the construction of an explicit renormalizable model with inclusion of flavor-gauge interactions is new. Within our framework, the constraints on DM are more severe compared to a generic

Effective Field Theory (EFT) analysis [6, 8]. In particular, the flavor constraints from new fermionic states, and the fact that the vacuum expectation values (vevs) of the flavon fields need to reproduce the quark masses, makes the structure of the theory much more rigid and predictive.

The paper is structured as follows. In Sec. III we derive general conditions for DM to be stabilized by the exact accidental flavor symmetry of the SM (flavor triality). An explicit realization of this possibility is introduced in Sec. III in the form of a model with fully gauged $\mathcal{G}_F^{\text{SM}}$. The resulting DM, flavor, and collider phenomenology is analyzed in detail in Sec. IV. We summarize our conclusions in Sec. VI, while more technical details of some of our computations are relegated to the Appendices.

II. STABILITY OF FLAVORED DARK MATTER

We start by formulating the general conditions required for flavored DM to be stable due to flavor triality. The SM exhibits a large global flavor symmetry $U(3)_Q \times U(3)_U \times U(3)_D \times U(3)_L \times U(3)_E$ in the limit of vanishing Yukawa interactions. In this paper we focus on the quark sector. This has the global symmetry $\mathcal{G}_F^{\text{SM}} \times U(1)_Y \times U(1)_B \times U(1)_{\text{PQ}}$. The three $U(1)$ factors are the hypercharge, baryon number (B), and the Peccei-Quinn symmetry, respectively. The remaining semisimple group is $\mathcal{G}_F^{\text{SM}} = SU(3)_Q \times SU(3)_U \times SU(3)_D$. The SM quarks transform under it as

$$Q_L \sim (3, 1, 1), \quad U_R \sim (1, 3, 1), \quad D_R \sim (1, 1, 3). \quad (1)$$

The $\mathcal{G}_F^{\text{SM}}$ global symmetry is broken by the SM Yukawa terms

$$\mathcal{L}_Y = \bar{Q}_L \tilde{H} y_u U_R + \bar{Q}_L H y_d D_R + \text{h.c.}, \quad (2)$$

where $\tilde{H} = i\sigma_2 H^*$. \mathcal{L}_Y is formally invariant under \mathcal{G}_F if $y_{u,d}$ are promoted to spurions that transform as $(3, \bar{3}, 1)$ and $(3, 1, \bar{3})$ [21, 24, 71–75]. NP is of MFV type if $y_{u,d}$ are the only flavor-breaking spurions also in the NP sector.

The SM Yukawa couplings in Eq. (2) break $U(1)_{\text{PQ}}$ and break $\mathcal{G}_F^{\text{SM}}$ to its center group \mathcal{Z}_3^{UDQ} , under which all three generations of quarks transform as

$\{U_R, D_R, Q_L\} \rightarrow e^{i2\pi/3}\{U_R, D_R, Q_L\}$. In the SM the \mathcal{Z}_3^{UDQ} is identical to a subgroup of $U(1)_B$. This is no longer true in the presence of NP. In MFV for instance, \mathcal{Z}_3^{UDQ} remains exact, while $U(1)_B$ can be broken, e.g., by dimension-9 operators [22] (see also [7]).

The \mathcal{Z}_3^{UDQ} may be the underlying reason for the stability of DM. To make this explicit it is useful to introduce \mathcal{Z}_3^X , a diagonal subgroup of $\mathcal{Z}_3^{UDQ} \times \mathcal{Z}_3^c$. Here, \mathcal{Z}_3^c is the center group of color $SU(3)_c$, under which $\{U_R, D_R, Q_L\} \rightarrow e^{-i2\pi/3}\{U_R, D_R, Q_L\}$. All the SM fields are thus \mathcal{Z}_3^X singlets. In MFV NP \mathcal{Z}_3^X is exact, so that the lightest \mathcal{Z}_3^X odd particle is stable and can be a DM candidate [7].

We generalize this observation beyond MFV. To this end, we introduce the notion of flavor triality [7]. Consider a field X in the $\mathcal{G}_F^{\text{SM}}$ representation $X \sim (n_Q^X, m_Q^X) \times (n_U^X, m_U^X) \times (n_D^X, m_D^X)$, where n_i^X, m_i^X are the Dynkin coefficients of the corresponding $SU(3)_i$ group. We call *flavor triality* the quantity

$$(n_X - m_X) \bmod 3, \quad (3)$$

where $n_X = n_Q^X + n_U^X + n_D^X$ and $m_X = m_Q^X + m_U^X + m_D^X$.

The basic requirements for flavored DM to be stable due to \mathcal{Z}_3^X are the following. First of all, $\mathcal{G}_F^{\text{SM}}$ needs to be a good symmetry in the UV. Secondly, $\mathcal{G}_F^{\text{SM}}$ needs to be broken only by spurions $\langle \Phi \rangle$ with zero flavor triality, $(n_{\langle \Phi \rangle} - m_{\langle \Phi \rangle}) \bmod 3 = 0$. This ensures that \mathcal{Z}_3^X is unbroken. (The spurions $\langle \Phi \rangle$ need to be color singlets in order not to break color.) The lightest \mathcal{Z}_3^X odd state is then stable. If it is a color singlet it is a potential DM candidate. This also means that DM is in a nontrivial flavor representation with nonzero flavor triality, $(n_\chi - m_\chi) \bmod 3 \neq 0$.

The above shows that models with flavored DM can deviate significantly from MFV. In particular, \mathcal{Z}_3^X is not broken by a vev of any field that is in an adjoint or in a bifundamental of $\mathcal{G}_F^{\text{SM}}$. Specifically, any function $f(y_u, y_d)$ leaves \mathcal{Z}_3^X unbroken. More generally, additional flavor-breaking sources that transform as $(8, 1, 1), (1, 3, \bar{3}), \dots$ may be present without spoiling DM stability. While the flavor structure of such NP models is not of MFV type in general, the stability of DM is still a consequence of an unbroken flavor subgroup. DM is in a nontrivial representation of the flavor group, leading to distinct phenomenology depending on the nature of the flavor breaking and on which flavor multiplet χ belongs to.

An important starting point in the above discussion was the assumption that $\mathcal{G}_F^{\text{SM}}$ is a good symmetry in the UV. This is most easily achieved, if $\mathcal{G}_F^{\text{SM}}$ is gauged. We explore this

possibility in the remainder of the paper.

III. GAUGED FLAVOR INTERACTIONS AND DARK MATTER

We gauge the full SM quark-flavor symmetry $\mathcal{G}_F^{\text{SM}}$. The fermionic sector is extended to cancel the anomalies of the new gauge sector. We use the model of Ref. [9] that allows for $\mathcal{O}(\text{TeV})$ flavor gauge bosons (FGBs). The SM Yukawas, $y_{u,d}$, arise from the vevs of new scalar fields transforming as

$$Y_u \sim (\bar{3}, 3, 1), \quad Y_d \sim (\bar{3}, 1, 3), \quad (4)$$

under $\mathcal{G}_F^{\text{SM}}$. The minimal set of chiral fermions that ensures anomaly cancellation of the new gauged sector is

$$\Psi_{uR} \sim (3, 1, 1), \quad \Psi_{dR} \sim (3, 1, 1), \quad \Psi_{uL} \sim (1, 3, 1), \quad \Psi_{dL} \sim (1, 1, 3), \quad (5)$$

where the index L and R represents their chirality. Together with the SM fermions they, therefore, form vector-like representations of $\mathcal{G}_F^{\text{SM}}$. The SM gauge quantum numbers of $\Psi_{uR}, \Psi_{dR}, \Psi_{uL}, \Psi_{dL}$ are the same as for U_R, D_R, U_R, D_R , respectively, i.e., they are $SU(2)_L$ singlets but charged under $U(1)_Y$. Because the new fermions are vector-like under the SM, e.g., Ψ_{uR} transforms like Ψ_{uL} under the SM, all anomalies in the SM sector cancel. Remarkably, with the above fermionic content also all mixed gauge anomalies cancel. In fact, one could also gauge two additional flavor diagonal $U(1)$'s, $U(1)_U$ and $U(1)_D$, as well as $U(1)_{B-L}$, a possibility that we do not pursue further, but is discussed in Ref. [9].

The Yukawa and relevant mass terms in the Lagrangian are [9]

$$\begin{aligned} \mathcal{L}_{\text{mass}} \supset & \lambda_u \bar{Q}_L \tilde{H} \Psi_{uR} + \lambda'_u \bar{\Psi}_{uL} Y_u \Psi_{uR} + M_u \bar{\Psi}_{uL} U_R \\ & + \lambda_d \bar{Q}_L H \Psi_{dR} + \lambda'_d \bar{\Psi}_{dL} Y_d \Psi_{dR} + M_d \bar{\Psi}_{dL} D_R + \text{h.c.}, \end{aligned} \quad (6)$$

where $\lambda_{u,d}^{(\prime)}$ are flavor-universal coupling constants and $M_{u,d}$ flavor-universal mass parameters. The mass terms in Eq. (6) mix the states $\Psi_{uL,uR}$ and $U_{L,R}$ forming mass eigenstates u_i and u'_i , where $i = 1, 2, 3$ is the generation index (and similarly for down-quark states). After electroweak symmetry breaking the masses for the two mass-eigenstate sets are, in the limit $m_{u'_i} \gg m_{u_i}$, [9, 23]

$$m_{u_i} \approx \frac{v}{\sqrt{2}} \frac{\lambda_u M_u}{\lambda'_u \langle Y_u \rangle_i}, \quad m_{u'_i} \approx \lambda'_u \langle Y_u \rangle_i. \quad (7)$$

The mass matrix for the FGBs, A_A^a , $A = Q, U, D$ and $a = 1, \dots, 8$, is governed by the vevs of the $Y_{u,d}$ scalar fields and the gauge couplings, [9, 23]

$$(\mathcal{M}_{AB}^2)_{ab} = \frac{1}{4} g_A g_B \text{Tr} [\langle Y_u \rangle \{ \lambda^a, \lambda^b \} \langle Y_u \rangle^\dagger] (\delta_{AB} \delta_{AQ} - 2\delta_{AQ} \delta_{BU} + Q \leftrightarrow U) + U, u \leftrightarrow D, d, \quad (8)$$

with λ^a the Gell-Mann $SU(3)$ matrices. The mass matrix is 24×24 dimensional. We denote the mass-ordered eigenstates by A^m , $m = 1, \dots, 24$, where A^{24} is the lightest one. The lightest gauge boson is found to be along the three diagonal λ_8 directions. This is a consequence of $\langle Y_u \rangle$ and $\langle Y_d \rangle$ being almost aligned and with very hierarchical eigenvalues, where the $\langle Y_u \rangle_{33}$ and $\langle Y_d \rangle_{33}$ are the smallest eigenvalues.

The SM Yukawas, $y_{u,d}$, are generated after $Y_{u,d}$ obtain a vev and the Ψ_i fields are integrated out. To first order in $M_{u,d}/\langle Y_{u,d} \rangle$, this gives

$$y_u \simeq \frac{\lambda_u M_u}{\lambda'_u \langle Y_u \rangle}, \quad y_d \simeq \frac{\lambda_d M_d}{\lambda'_d \langle Y_d \rangle}. \quad (9)$$

The SM Yukawas, $y_{u,d}$, are non-analytic functions of the spurions $\langle Y_{u,d} \rangle$, which signals that the theory is strictly speaking not MFV. Analogously, the NP states, u'_i, d'_i and A^m , have masses that are non-analytic in terms of the SM Yukawas. However, the low-energy observables, with only the SM fields on the external legs can be MFV-like. If the $M_{u,d}/\langle Y_{u,d} \rangle$ suppressed terms are kept in Eq. (9), the $y_{u,d}$ become more involved functions of $\langle Y_{u,d} \rangle^{-1}$. These are analytic in $\langle Y_{u,d} \rangle^{-1}$ since the effects of NP states decouple in the $\langle Y_{u,d} \rangle \rightarrow \infty$ limit. Similarly, the NP contributions to the low-energy observables C_i take the form $\delta C_i = F(\langle Y_u \rangle^{-1}, \langle Y_d \rangle^{-1}) = \tilde{F}(y_u, y_d)$, with F, \tilde{F} analytic functions. One can thus expand $\delta C_i = a_1 y_u y_u^\dagger + a_2 (y_u y_u^\dagger)^2 + b_1 y_u y_u^\dagger y_d y_d^\dagger + \dots$, where we assumed for illustration that the transition is due to the left-handed quark current. As long as there are no large flavor-conserving ratios, i.e., as long as $(\lambda_u M_u / \lambda'_u) / (\lambda_d M_d / \lambda'_d) \ll 1/|V_{cb}|$, the Taylor expansion can be truncated after a few terms (see Ref. [24] for a more detailed discussion). In this limit, the low-energy effects are of the MFV type, suppressing the FCNCs to acceptable levels already for NP states at the electroweak scale. In a numerical analysis that we perform in Appendix A, we find that the expansion of the effective weak Hamiltonian in terms of SM Yukawa couplings can indeed still be performed for FGB contributions.

Since $\langle Y_{u,d} \rangle$ are in the bifundamental representation of $\mathcal{G}_F^{\text{SM}}$, the \mathcal{Z}_3^X remains unbroken. As argued above the \mathcal{Z}_3^X can be used to make flavored DM candidates stable. We consider two examples: i) a fermionic DM in a vector-like representation of $\mathcal{G}_F^{\text{SM}}$ that thermalizes

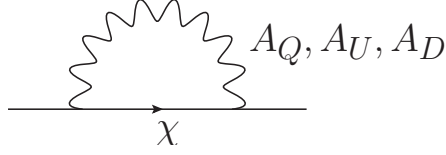


Figure 1: Radiative corrections due to FGBs, A_Q, A_U, A_D , split the DM multiplet χ .

with the visible sector through FGBs, and ii) a scalar flavored DM, that interacts with the visible sector by exchanging FGBs as well as the Higgs.

A. Fermionic flavored dark matter

The DM in the first model is a massive Dirac fermion, χ , in a vector-like representation of $SU(3)_U$,

$$\chi \sim (1, 3, 1), \quad (10)$$

so that no gauge anomalies are induced. Its mass term is

$$\mathcal{L}_{\text{mass}}^\chi = m_\chi^0 \bar{\chi} \chi. \quad (11)$$

Since χ is charged under \mathcal{Z}_3^χ , the lightest member of the χ triplet is stable. Note that we could also gauge a larger global group $\mathcal{G}_F^{SM} \times SU(3)_\chi$, with χ transforming under $SU(3)_\chi$. That we identify $SU(3)_\chi$ with $SU(3)_U$ is a model-building choice.

The DM flavor triplet, χ , is split by radiative corrections due to the exchanges of FGBs, see Fig. 1. In the $m_\chi^0 \ll m_A$ limit, the DM mass splitting at one-loop is given by

$$\Delta m_\chi = -\frac{3}{4} \frac{g_U^2}{16\pi^2} m_\chi^0 \left(\Xi - \frac{1}{3} \text{Tr } \Xi \right), \quad (12)$$

where Δm_χ is a 3×3 matrix and so is $\Xi \equiv \lambda^a (\log \mathcal{M}_A^2 / \mu^2)^{ab} \lambda^b$. The FGB mass matrix \mathcal{M}_A^2 is given in Eq. (8), while the a, b indices run only over the eight $SU(3)_U$ generators. The unphysical μ dependence cancels in the r.h.s. of Eq. (12). The χ_i , $i = 1, 2, 3$, mass eigenstates are obtained by diagonalizing the mass matrix Δm_χ . And Ξ is a function of $Y_u^\dagger Y_u$ and $Y_u^\dagger Y_d Y_d^\dagger Y_u$ vev combinations, making the χ mass eigen-basis slightly misaligned with respect to the up-quark one. The χ_1 mass receives contributions from the heaviest FGBs (cf. section V). The lightest state is thus χ_1 , i.e., with the predominantly up-quark flavor, while the heaviest is the top-flavored state, χ_3 .

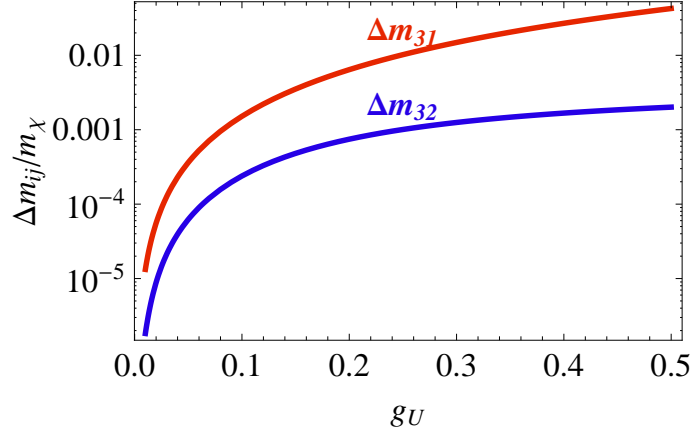


Figure 2: Typical radiative splitting of the fermionic DM multiplet with Δm_{31} (Δm_{32}) shown in red (blue) as a function of g_U , while all other parameters are kept fixed at $g_Q = 0.4, g_D = 0.5$, $M_u = 600 \text{ GeV}$, $M_d = 400 \text{ GeV}$, $\lambda_u = 1$, $\lambda'_u = 0.5$, $\lambda_d = 0.25$, $\lambda'_d = 0.3$.

In the numerics we use the exact one-loop expressions for the DM mass splitting,

$$\Xi = \frac{3}{2} \lambda^a \mathcal{W}^{a+8,m} [B_1(m_\chi^2, m_{A_m}^2, m_\chi^2) - B_0(m_\chi^2, m_{A_m}^2, m_\chi^2)] \mathcal{W}^{\dagger m, c+8} \lambda^c. \quad (13)$$

Summation over FGB mass eigenstate indices $m = 1, \dots, 24$ and over $a, c = 1, \dots, 8$ is understood. The 24×24 dimensional matrix \mathcal{W} diagonalizes the gauge-boson mass matrix and $B_{0,1}$ are the Veltman-Passarino functions. Typical values of the mass splitting as a function of g_U are shown in Fig. 2. Denoting $\Delta m_{ij} \equiv m_{\chi_i} - m_{\chi_j}$, we see that $\Delta m_{32} \ll \Delta m_{31}$, so that the lightest state χ_1 is split away from χ_2 and χ_3 , with the latter approximately degenerate, $m_{\chi_2} \simeq m_{\chi_3}$. This is very different from MFV DM [6–8] where the DM mass splitting is assumed to be expandable in the SM Yukawa couplings. In that case one has an approximate $U(2)$ symmetry for the first two generations giving $m_{\chi_1} \simeq m_{\chi_2}$, while the top-flavored DM, χ_3 , is split away from the first two generations, and can be either significantly heavier or lighter.

The relation $\Delta m_{32} \ll \Delta m_{31}$ signifies that our flavored DM is non-MFV. The flavor gauge group $SU(3)_U$ is broken by the FGB vevs $\langle Y_u \rangle$. This breaking is larger in the first two generations. Since the quark masses are inversely proportional to $\langle Y_u \rangle$, this leads to an approximate global $U(2)_U$ symmetry in the quark sector. Such an approximate symmetry is not found for the radiative corrections to DM masses, m_{χ_i} . The DM multiplet has a chiral symmetry in the limit $m_\chi \rightarrow 0$ ensuring that the radiative corrections are proportional to m_χ and only log-dependent on FGB masses. The splitting does not vanish in the $\langle Y_u \rangle \rightarrow \infty$

limit (or, equivalently, $y_u \rightarrow 0$ limit), since in this limit the $SU(3)_U$ gauge group is still completely broken. Numerically, for $m_\chi \sim \text{TeV}$ the splittings are $\Delta m_{31} \sim \mathcal{O}(10 \text{ GeV})$ and $\Delta m_{32} \sim \mathcal{O}(1 \text{ GeV})$ for $g_U \sim 0.4$ and can be less than a pion mass for an order of magnitude smaller g_U .

The DM multiplet can be split more significantly if there is flavor breaking beyond $\langle Y_u \rangle$, $\langle Y_d \rangle$. As an example we consider an additional scalar field in the adjoint of $SU(3)_U$, $\Phi_U \sim (1, 8, 1)$. The DM mass Lagrangian now reads

$$\mathcal{L}'_{\text{mass}} = m_\chi^0 \bar{\chi}_L \chi_R + \lambda_\chi \bar{\chi}_L \Phi_U \chi_R + \text{h.c.}, \quad (14)$$

and yields DM masses that are split already at tree level, $\Delta m_\chi = \lambda_\chi \langle \Phi_U \rangle$. We assume that $\langle \Phi_U \rangle$ is aligned with $Y_U^\dagger Y_U$. Then the two diagonalize in the same basis giving $\mathcal{O}(1)$ splitting between all three members of the multiplet. The alignment is not needed in general, but does simplify our analysis. For the same reason, we also take the first state to be the lightest one, $m_{\chi_1} < m_{\chi_{2,3}}$.

The χ_i interact with the SM through FGBs. This also induces the decay of the heavier two states in the DM multiplet, $\chi_{2,3}$, to χ_1 . We parametrize the relevant interactions with

$$\begin{aligned} \mathcal{L}_\chi \supset & (\hat{g}_\chi^m)_{ij} \bar{\chi}_i \gamma^\mu \chi_j A_\mu^m \\ & + \bar{u}_k \gamma^\mu \left((\hat{\mathcal{G}}_R^u)_{kl,m} P_R + (\hat{\mathcal{G}}_L^u)_{kl,m} P_L \right) u_l A_\mu^m \\ & + \bar{d}_k \gamma^\mu \left((\hat{\mathcal{G}}_R^d)_{kl,m} P_R + (\hat{\mathcal{G}}_L^d)_{kl,m} P_L \right) d_l A_\mu^m, \end{aligned} \quad (15)$$

where $P_{R,L} \equiv \frac{1}{2}(1 \pm \gamma^5)$ and $k, l = 1, \dots, 6$. The couplings of χ_i to the gauge bosons are

$$(\hat{g}_\chi^m)_{ji} = \left(-\frac{1}{2} g_U U^\dagger \lambda_n^U \mathcal{W}^{nm} U \right)_{ji}, \quad (16)$$

where U diagonalizes the m_χ mass matrix, $U^\dagger m_\chi U = \hat{m}_\chi$, and \mathcal{W} diagonalizes the gauge-boson mass matrix. The explicit form of FGB couplings to exotic and SM quarks, $(\hat{\mathcal{G}}_{L/R}^{u/d})_{kl,m}$, can be found in Appendix A.2 of Ref. [23].

The partial decay width for $\chi_i \rightarrow \chi_j q_l \bar{q}_k$ is, neglecting hadronization effects,

$$\Gamma(\chi_i \rightarrow \chi_j q_l \bar{q}_k) = \frac{3}{(2\pi)^3} \frac{\Delta m_{ij}^5}{15} \left[\left| \sum_m (\hat{g}_\chi^m)_{ij} \frac{1}{m_{A^m}^2} (\hat{\mathcal{G}}_L^u)_{kl,m} \right|^2 + L \rightarrow R \right], \quad (17)$$

where the sum runs over the FGB mass eigenstates $m = 1, \dots, 24$. Expression (17) is valid in the $|\Delta m_{ij}| \ll m_{\chi_i}$ limit, and neglecting the quark masses. The above approximations are

valid for all the values of parameter for which the correct relic abundance is obtained and the FCNC, collider and direct DM detection constraints are satisfied.

If the mass splitting is less than the pion mass the decay $\chi_i \rightarrow \chi_j q_l \bar{q}_k$ is kinematically not allowed. The heavier χ_i states then decay radiatively to $\chi_i \rightarrow \chi_j \gamma \gamma$. For our purposes an order of magnitude estimate of the decay width suffices. The naive dimensional analysis estimate gives

$$\Gamma(\chi_i \rightarrow \chi_j \gamma \gamma) \sim \frac{\Delta m_{ij}^9}{8\pi} \frac{1}{16\pi^2} \left(\frac{\alpha}{4\pi}\right)^2 \left[\left| \sum_{m,f} \frac{(\hat{g}_\chi^m)_{ij}}{m_{A^m}^2} \frac{Q_u^2}{m_f^2} \left((\hat{\mathcal{G}}_L^u)_{ff,m} - (\hat{\mathcal{G}}_R^u)_{ff,m} \right) \right|^2 + u \rightarrow d \right], \quad (18)$$

where $Q_u = 2/3$ and $Q_d = -1/3$ are the electromagnetic charges of up and down quarks. The sum over m runs over the FGB mass eigenstates, while the sum over f is over the SM quarks and exotic states, of mass m_f (for up, down and strange quarks this needs to be replaced with Λ_{QCD}).

B. Scalar flavored dark matter

The second model has scalar DM, ϕ , in a fundamental representation of $SU(3)_U$

$$\phi \sim (1, 3, 1). \quad (19)$$

The main difference with the fermionic flavored DM from the previous subsection is that the scalar DM interacts with the visible sector via two different types of interactions. The first is its couplings to the FGBs, which is similar to the case of the fermionic DM. The second is a direct coupling to the Higgs

$$\mathcal{L}_{\text{int}}^{\text{DM}} = \lambda_H (\phi^\dagger \phi) (H^\dagger H). \quad (20)$$

For a thermal relic the DM annihilations proceed predominantly through the Higgs portal. The interactions via FGBs are subdominant except if $m_\phi \simeq m_{A^a}/2$ for some A^a . Unless this is the case, the fact that the DM carries a flavor quantum number is exhibited only through the multiplicity of the states.

After electroweak symmetry breaking, the DM–Higgs interactions are given by

$$\mathcal{L}_{\text{int}}^{\text{DM}} \supset \lambda_H (vh + v^2/2) \phi^\dagger \phi, \quad (21)$$

and the DM mass term $m_0^2 \phi^\dagger \phi$ is shifted by the Higgs condensate to give the DM mass of

$$m_\phi^2 = m_0^2 + v^2/2. \quad (22)$$

The vevs of the flavons, $\langle Y_u \rangle$ and $\langle Y_d \rangle$, split the DM multiplet at tree level through

$$\mathcal{L} \supset \kappa_1 (\phi^\dagger \lambda^a \phi) \text{Tr}(Y_u^\dagger \lambda^a Y_u) + \kappa_2 (\phi^\dagger \{\lambda^a, \lambda^b\} \phi) \text{Tr}(Y_u^\dagger \{\lambda^a, \lambda^b\} Y_u). \quad (23)$$

The spectrum is also split by radiative corrections due to FGBs. These are quadratically divergent and proportional to the square of the FGB mass. In principle, it is possible to fine tune the tree-level and loop contributions to give almost degenerate DM flavor multiplet. However, given the hierarchical FGB masses, it is more likely that the DM multiplet is split completely, and only the lightest state is relevant for DM phenomenology. Depending on the signs of κ_i in Eq. (23) the lightest ϕ component can be either top-quark or up-quark flavored. We choose the latter option in the numerics for easier comparison with the fermionic case.

IV. DARK MATTER AND NEW PHYSICS PHENOMENOLOGY

We turn next to the phenomenology of the flavored DM models. We perform a scan over the parameters of the models and show that the lowest DM states, both for the fermionic DM, χ , and the scalar DM, ϕ , can be thermal relics. To make the scan numerically tractable we rely on several approximations in calculating the relic density, which we explain below. We also discuss the predictions for direct DM detection, and the constraints from FCNCs and collider searches.

A. Scan results

In the scan we fix $\lambda_u = 1$ and vary $\lambda_d \in [1/(4\pi), 1]$. The range is chosen with the expectation that one will be able to accommodate both the SM top and bottom quark Yukawas as well as satisfy electroweak precision constraints and direct t' and b' searches [9]. In addition we vary conservatively $\lambda'_{u,d} \in [1/(4\pi)^2, 4\pi]$, $g_{Q,U,D} \in [1/(4\pi)^2, 4\pi]$, and $M_{u,d} \in [0.2, 20]$ TeV. To a good approximation, the variation of M_u effectively compensates the fact that we do not vary λ_u as seen from Eq. (9). We have verified that further extending these parameter ranges does not extend the viable DM-model parameter space. For instance, the upper

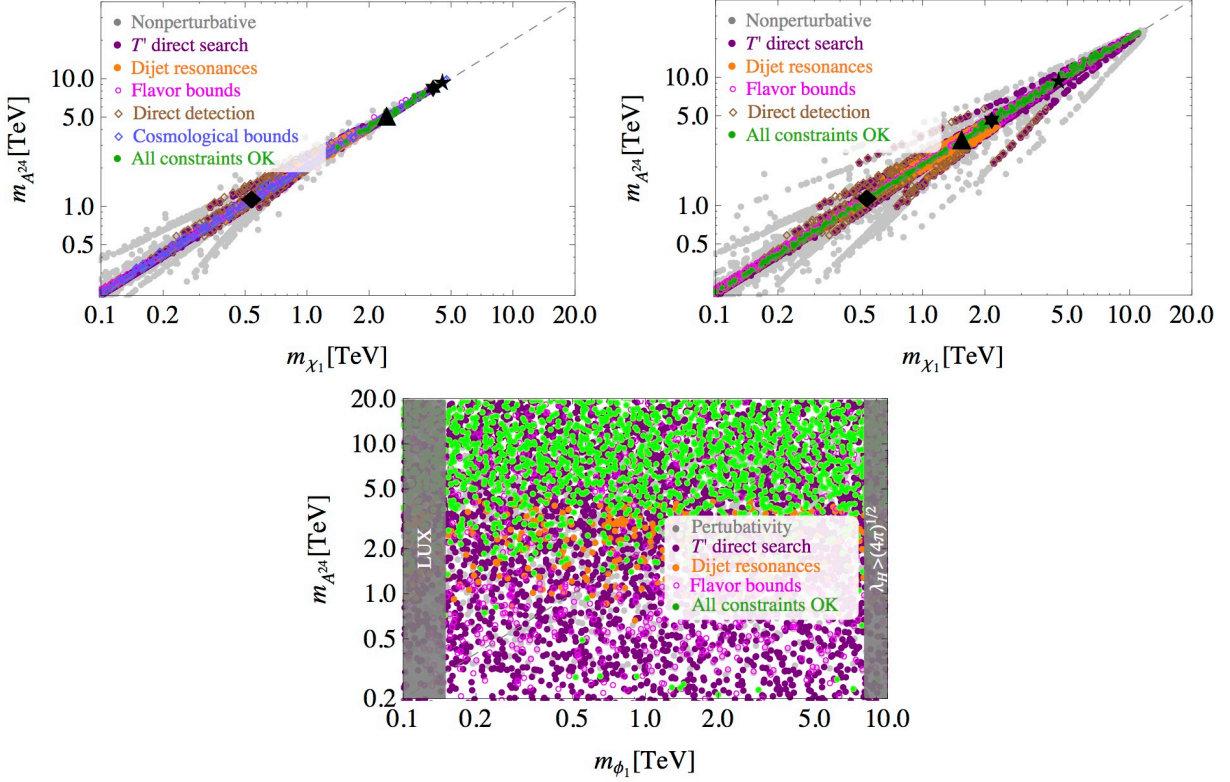


Figure 3: The results of the scan for fermionic DM with radiative mass splitting (upper left panel), in the large mass splitting limit (upper right panel) and scalar (lower panel) flavored DM. Constraints from perturbativity (grey), t' (dark magenta) and dijet resonance (orange) searches, flavor bounds (light magenta), early-time cosmology (blue) and direct DM detection (brown) are consecutively applied. Allowed parameter points are denoted by green. For scalar flavor DM (right) we show the LUX and perturbativity bounds as two grey bands. The four benchmark points for fermionic flavored DM are denoted by a diamond, a triangle, a hexagon and a pentagon.

ranges of $g_{Q,U,D}$ and $\lambda'_{u,d}$ already lie in the non-perturbative regime. To ensure perturbative control we require that all the FGB decay widths satisfy $\Gamma_{A^m} < 0.5 m_{A^m}$, and that the radiative mass splitting for the fermionic DM is $|\Delta m_{ij}| < 0.5 m_\chi$. This imposes upper bounds on $g_{Q,U,D}$ that are typically close to $\sqrt{4\pi}$. Similar constraints on $\lambda'_{u,d}$ are expected to follow from analogous considerations in the flavored Higgs sector, i.e., by requiring the total widths of the flavored scalars $Y_{u,d}$ to be small compared to their masses.

The results of the scan are shown in Figs. 3, 4, 5. Fig. 3 (upper panels) show the results of the scan for fermionic DM model with radiative (left) and large tree-level mass

splitting (right). Fig. 3 (lower panel) instead shows the results of the scan for scalar DM. All the points shown in Fig. 3 give the correct relic DM abundance, Ω_{DM} . Different colors denote consecutively applied constraints. The grey points fail the perturbativity requirement, $\Gamma_{A^m} < 0.5 m_{A^m}$, $|\Delta m_{ij}| < 0.5 m_\chi$ discussed above. The points in brown are excluded by direct DM detection, the points in dark magenta by t' direct searches and the points in orange by dijet resonance searches. The flavor bounds exclude points in light magenta, while cosmological considerations – mainly from big bang nucleosynthesis – exclude points in dark blue. The green points are allowed by all constraints. In Figs. 4 and 5 we also show the points where it is not possible to obtain the correct relic abundance (denoted by light blue), and denote by dark red the points excluded by the combined direct-detection, collider and flavor constraints.

For fermionic DM the observed relic abundance requires resonantly enhanced annihilation through s -channel exchange of the lightest FGB, A^{24} , see Fig. 6 (left). This leads to the correlation $m_{\chi_i} \simeq m_{A^{24}}/2$ shown in Fig. 3 (upper panels). It is possible to obtain the correct relic abundance also if the DM mass is only approximately half of the lightest FGB (points away from the diagonal in Fig. 3 (upper panels)). These points require at least some of the couplings to be large and are excluded by flavor, collider, direct detection, or perturbativity constraints. For the allowed points the relation $m_{\chi_i} \simeq m_{A^{24}}/2$ is satisfied to within a few decay widths of A^{24} , i.e. to within $\mathcal{O}(10\%)$. The scalar flavored DM, on the other hand, predominantly annihilates through the Higgs portal, see Fig. 6 (right). There is thus no relation between m_ϕ and $m_{A^{24}}$, as seen in Fig. 3 (lower panel).

In the remainder of this section we discuss how the various constraints on the DM model were obtained.

B. Thermal relic

For the calculation of the DM relic density we follow Refs. [25, 26]. To speed-up the numerical scan we work in the non-relativistic limit, using the freeze-out approximation. The details of the calculation are given in Appendix B. Among viable parameter points we choose four benchmarks that satisfy all other experimental constraints. For the benchmark points we verify the DM relic abundance calculation using the MadDM [27] package. We computed the required Feynman rules using the Feynrules [28] package.

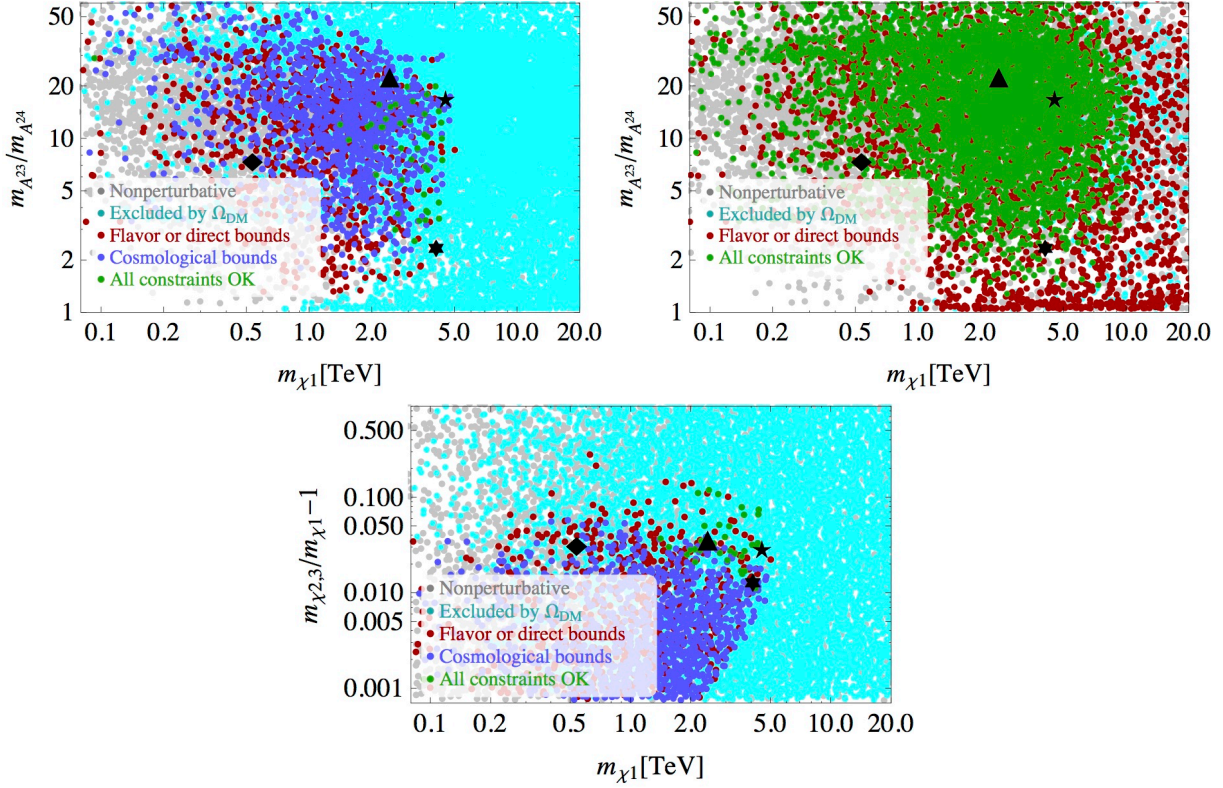


Figure 4: The ratio of masses of the next-to-lightest to the lightest FGBs, $m_{A^{23}}/m_{A^{24}}$ for radiatively split DM multiplet (upper left panel), and for the large mass splitting limit (upper right panel), as functions of the DM mass, m_{χ_1} , for the fermionic flavored DM. Lower panel shows the relative radiative mass splitting in the DM multiplet. The constraints due to perturbativity (grey), too large relic abundance (light blue), early cosmology (dark blue), flavor and direct bounds (dark red), are applied consecutively, leaving allowed points (green).

1. Fermionic dark matter

In the fermionic DM model the DM annihilation to quarks is dominated by s -channel exchange of the lightest FGB, A^{24} , see Fig. 6 (left panel). The $\chi_i \bar{\chi}_i \rightarrow \bar{u}_j u_j$ annihilation cross section is given by

$$\sigma(\chi_i \bar{\chi}_i \rightarrow \bar{u}_j u_j) \simeq \frac{(\hat{g}_{\chi}^{24})_{ii}^2}{4\pi} \frac{s^{1/2} (s + 2m_{\chi_i}^2)}{\sqrt{s - 4m_{\chi_i}^2}} \frac{(\hat{\mathcal{G}}_V^u)_{jj,24}^2 + (\hat{\mathcal{G}}_A^u)_{jj,24}^2}{(s - m_{A^{24}}^2)^2 + m_{A^{24}}^2 \Gamma_{A^{24}}^2}, \quad (24)$$

where

$$\hat{\mathcal{G}}_{V,A}^u = (\hat{\mathcal{G}}_L^u \pm \hat{\mathcal{G}}_R^u)/2, \quad (25)$$

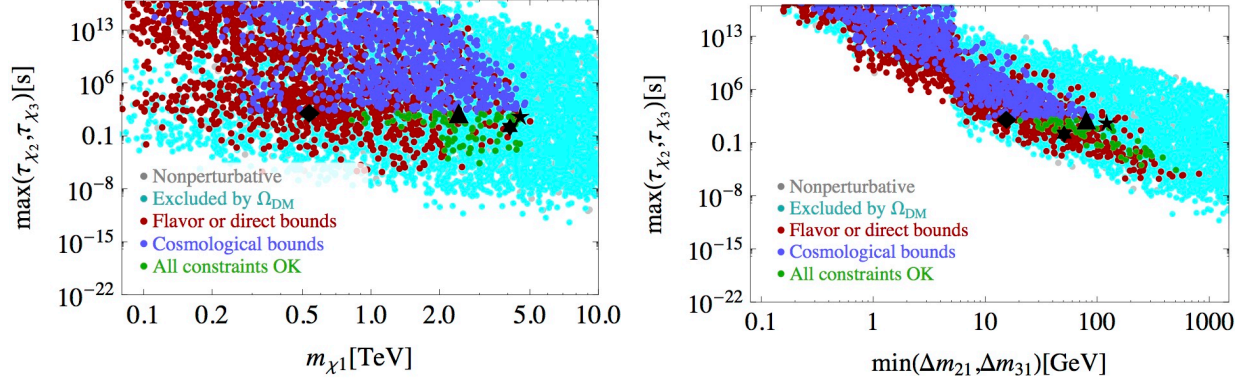


Figure 5: The maximal decay time of the two heavy states in the DM multiplet as functions of DM mass (left) and the minimal mass splitting in the DM multiplet (right) for radiatively split fermionic flavored DM. The color coding is as in Fig. 4.



Figure 6: The Feynman diagrams for the dominant processes in the DM annihilation for fermionic (left) and scalar (right) flavored DM. For scalar DM only one representative diagram is shown; other relevant final states include $b\bar{b}, c\bar{c}, \tau\tau$ and $t\bar{t}, hh, ZZ$ (when kinematically allowed).

\sqrt{s} is the center of mass energy and $\Gamma_{A^{24}}, m_{A^{24}}$ are the decay width and mass of the lightest FGB, respectively. In Eq. (24) we have neglected quark masses; the full expression is given in Eq. (B8). The $\chi_i \bar{\chi}_i \rightarrow \bar{d}_j d_j$ annihilation cross section follows from Eq. (24) by replacing $u \rightarrow d$. The full decay width of the lightest FGB is the sum of all partial decay widths for kinematically allowed channels,

$$\Gamma(A^{24} \rightarrow \bar{u}_j u_j) \simeq \frac{m_A^{24}}{4\pi} \left((\hat{\mathcal{G}}_V^u)_{jj,24}^2 + (\hat{\mathcal{G}}_A^u)_{jj,24}^2 \right). \quad (26)$$

In the above expression we have neglected the quark masses for simplicity, with the full expression given in Eq. (B9). The rates for $A^{24} \rightarrow \chi_i \bar{\chi}_i, \bar{d}_j d_j$ are obtained by trivial coupling replacements and by correcting the color multiplicity factors.

The correct relic abundance requires resonant annihilation, $m_\chi \simeq m_{A^{24}}/2$, see Fig. 3 (upper panels). This implies an upper bound on the DM mass through the following argument. The thermally averaged DM annihilation cross section scales in the narrow width approximation as

$$\langle\sigma v\rangle \propto \frac{g_{A^{24}}^4}{m_{A^{24}}\Gamma_{A^{24}}} + \mathcal{O}(\Gamma_{A^{24}}/m_{A^{24}}) \sim \frac{1}{\langle Y\rangle_{A^{24}}^2}. \quad (27)$$

Here, we used the approximate scaling for the FGB masses and decay widths, $m_{A^{24}} \sim \langle Y\rangle_{A^{24}}g_{A^{24}}$, $\Gamma_{A^{24}} \sim (g_{A^{24}})^2m_{A^{24}}$. The $\langle Y\rangle_{A^{24}}$ and $g_{A^{24}}$ are, respectively, the projections of the $Y_{u,d}$ vevs and $g_{Q,U,D}$ couplings onto the lightest FGB, A^{24} . The DM relic abundance is $\Omega_{\text{DM}} \propto 1/\langle\sigma v\rangle \propto \langle Y\rangle_{A^{24}}^2$ and thus depends predominantly only on the flavon vevs. Not exceeding the relic abundance puts an upper bound $\langle Y\rangle_{A^{24}} \lesssim \mathcal{O}(\text{few } 100 \text{ GeV})$, almost independent of the DM mass. Since $m_{A^{24}} \sim \langle Y\rangle_{A^{24}}g_{A^{24}}$, and $g_{A^{24}} \lesssim \sqrt{4\pi}$ for the theory to be perturbative, this also sets an upper bound on the lightest FGB mass. This in turn implies an upper bound on the DM mass through the relation $m_\chi \simeq m_{A^{24}}/2$.

In the limit where only χ_1 contributes to the DM relic abundance we find, using the scan, an upper bound $m_{\chi_1} \lesssim 10 \text{ TeV}$. The approximation is valid if $\chi_{2,3}$ states decay well before χ_1 freezes out (i.e. $\tau_{\chi_{2,3}} \lesssim 10^{-11} \text{ s}$ for $m_\chi \sim 1 \text{ TeV}$). For purely radiative DM mass splitting this is never the case (c.f. Fig. 5). Instead, if $\chi_{2,3}$ decay after decoupling, they will also contribute to the final DM relic abundance and one needs to sum all three contributions. In this case, the constraints on the mass spectrum become much more severe. In particular, in order for all χ components to annihilate efficiently their masses need to be within a few decay widths away from the lightest FGB (LFGB) mass. This in turn implies that the (radiative) DM mass splitting has to be of the order of the LFGB width. Since the splitting increases with g_U we expect these effects to decrease the effective thermal DM annihilation cross section much before the theory becomes non-perturbative. Indeed we find, using the scan, an upper bound $m_{\chi_1} \lesssim 5 \text{ TeV}$.

Fig. 4 (upper panels) shows the ratio of masses of the next-to-lightest and the lightest FGB, $m_{A^{23}}/m_{A^{24}}$, as a function of DM mass m_{χ_1} for radiatively split DM multiplet (left) and in the large mass splitting limit (right). In most of the parameter space satisfying the Ω_{DM} constraint A^{23} is much heavier than A^{24} so that the effects of higher resonances are indeed negligible. This justifies the use of only the lightest FGB when calculating the DM density in the scan.

Fig. 4 (lower panel) shows the relative radiative mass splitting $\Delta m_{21}/m_{\chi_1}$ and $\Delta m_{31}/m_{\chi_1}$

as a function of the DM mass, m_{χ_1} (both splittings are shown in one plot). In most cases the mass splitting is below $\mathcal{O}(10\%)$ in order for all χ components to lie close to the resonant condition, as anticipated.

2. Scalar dark matter

For scalar DM the interactions with the visible sector are mainly due to the Higgs-portal operator, $\lambda_H(\phi^\dagger\phi)(H^\dagger H)$, in Eq. (20). The interactions due to the exchanges of FGBs are subleading except for the resonant annihilation regions $m_{\phi_1} \simeq m_{A^{24}}/2$. By adjusting the value of λ_H one can obtain the correct relic abundance for any mass of m_{ϕ_1} irrespective of the lightest FGB mass, $m_{A^{24}}$, see Fig. 3 (bottom panel). In the calculation of the thermal relic abundance we include the following annihilation channels: $\phi_1^\dagger\phi_1 \rightarrow \bar{b}b, \bar{c}c, \tau^+\tau^-, W^+W^-, ZZ, hh$ and $\bar{t}t$, see Fig. 6. The annihilation cross sections are

$$\sigma(\phi_1^\dagger\phi_1 \rightarrow \bar{f}f) = \frac{\lambda_H^2 m_f^2 N_c (1 - 4m_f^2/s)^{3/2}}{8\pi \sqrt{1 - 4m_{\phi_1}^2/s} [(m_h^2 - s)^2 + m_h^2 \Gamma_h^2]}, \quad (28)$$

$$\sigma(\phi_1^\dagger\phi_1 \rightarrow VV) = \frac{c_V \lambda_H^2 \sqrt{1 - 4m_V^2/s} (12m_V^4 - 4m_V^2 s + s^2)}{16\pi s \sqrt{1 - 4m_{\phi_1}^2/s} [(m_h^2 - s)^2 + m_h^2 \Gamma_h^2]}, \quad (29)$$

where $c_W = 1$, $c_Z = 1/2$ and

$$\sigma(\phi_1^\dagger\phi_1 \rightarrow hh) = \frac{\lambda_H^2 \sqrt{1 - 4m_h^2/s} [(2m_h^2 + s)^2 + m_h^2 \Gamma_h^2]}{32\pi s \sqrt{1 - 4m_{\phi_1}^2/s} [(m_h^2 - s)^2 + m_h^2 \Gamma_h^2]}. \quad (30)$$

The thermally averaged cross sections and relic abundances are computed following the prescription described in Appendix B. The results of the scan are given in Fig. 3 (bottom panel). In Fig. 7 we plot the coupling λ_H necessary to obtain correct DM relic density as a function of the DM mass, m_{ϕ_1} . As commented in Sec. IIIB the flavon vevs split the lightest DM state ϕ_1 from the heavier ones, such that only ϕ_1 contributes to Ω_{DM} (lower dashed line). Instead, if the splitting is too small for $\phi_{2,3}$ to decay before freeze-out, all three components contribute (upper dashed line). In both cases, requiring the Higgs-portal coupling $\lambda_H < \sqrt{4\pi}$, such that the relic-abundance calculation is well in the perturbative regime, limits the DM mass $m_{\phi_1} \lesssim 8 \text{ TeV}$.

Note that the role of the Higgs portal may be played by other light scalars. In Ref. [20] the flavon field of the Abelian horizontal symmetry was used to enhance the DM annihilation cross section. If the flavons are light, they can also modify the phenomenology of

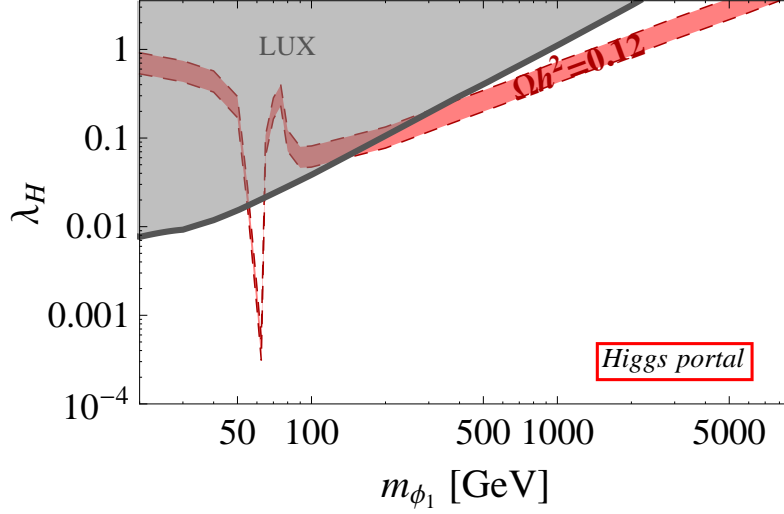


Figure 7: The Higgs–DM coupling, λ_H , as a function of DM mass that gives the correct relic abundance for the Higgs portal scalar DM (red band). The upper (lower) dashed edge corresponds to the limit where $\phi_{2,3}$ decay much after (before) the thermal freeze-out of ϕ_1 . The LUX bound, assuming correct relic abundance, is shown as a shaded grey region.

the fermionic flavored DM, allowing DM annihilation into flavons. In this case the DM phenomenology of the fermionic flavored DM would be closer to the one of our scalar DM model.

C. Cosmology

The heavier flavored DM states, both for the fermionic DM, $\chi_{2,3}$, and scalar DM, $\phi_{2,3}$, are unstable. They decay through the $\chi_i \rightarrow \chi_j \bar{q} q'$ transition when the mass splitting is larger than the pion mass, and through the $\chi_i \rightarrow \chi_j \gamma \gamma$ otherwise, cf. Eqs. (17), (18). The SM particles in the final state of these decays can have various observable effects in cosmology and astrophysics.

The two relevant sets of parameters are the lifetimes of the two heavy states, $\tau_{\chi_{2,3}}$, and the related mass splittings of the DM multiplet (with respect to the lightest state), $\Delta m_{31}, \Delta m_{21}$. The lifetimes determine at which cosmological epoch the heavy states decay. The mass splittings control the released combined electromagnetic and hadronic energy, $E_{\text{vis}} \simeq \Delta m_{21,31}$.

They also determine the relic abundances of the heavy states. Generically, near the degenerate limit each state contributes roughly a third of the total DM relic abundance, Ω_{DM} . Close to the resonant condition $m_\chi \simeq m_{A^{24}}/2$ the $\chi_{1,2,3}$ relic abundances may differ from $\Omega_{\text{DM}}/3$, depending on the common DM mass and relative mass splittings.

For the scalar DM the mass splitting is expected to be large. The $\phi_{2,3}$ therefore decay before primordial nucleosynthesis. The decays yield negligible entropy release due to the small $\phi_{2,3}$ abundances. Such scenarios are basically unconstrained by current cosmological observations. The same is true for the fermionic DM if additional spurions split the DM multiplet at tree level.

If the fermionic DM multiplet is split solely by radiative corrections, the $\chi_{2,3}$ and χ_1 are generically much more degenerate, cf. Fig. 4 (right). The $\chi_{2,3}$ states are then potentially long lived. For $\tau_{2,3} \sim \mathcal{O}(10^{-1} \text{ s} - 10^{12} \text{ s})$ the decays may affect the primordial generation of light nuclear elements [29]. For longer lifetimes, $\tau_{2,3} \sim \mathcal{O}(10^{10} \text{ s} - 10^{13} \text{ s})$, the $\chi_{2,3}$ decays distort the thermalization of the CMB by injecting high-energy photons into the plasma before recombination, which is strongly constrained [30, 31]. The $\chi_{2,3}$ states with lifetimes longer than $\tau_{2,3} \gtrsim 10^{10} \text{ s}$ are ruled out, if the injected photons carry energy above the thresholds of the efficient thermalization processes. Typically this is a fraction of the electron mass. For even longer lifetimes, $\tau_{2,3} \gtrsim 10^{13} \text{ s}$, the $\chi_{2,3}$ states decay after recombination. This results in photons that free-stream to us and can be searched for in diffuse galactic and extragalactic gamma and X-ray spectra. A combination of measurements excludes scenarios with $\tau_{2,3} \lesssim 10^{26} \text{ s}$ all the way down to $\Delta m_{21,31} \gtrsim \mathcal{O}(10) \text{ keV}$ [32].

In the remainder of this section we consider in more detail the region $\tau_{\chi_{2,3}} \sim 10^{-1} \text{ s} - 10^{12} \text{ s}$, where the big bang nucleosynthesis (BBN) provides the most stringent constraints [29, 33]. The injection of energetic photons or hadrons from $\chi_{2,3}$ decays during or after BBN adds an additional non-thermal component to the plasma that can modify the abundances of the light elements [34–38]. The bounds differ depending on whether the decays result in hadronic or electromagnetic showers in the plasma. The most stringent bounds are for a relic that produces mostly hadronic showers. This is because the electromagnetically interacting particles such as photons and electrons thermalize very quickly by interacting with the tail of the CMB distribution until the universe is 10^6 s old. In our case, the decays $\chi_{2,3} \rightarrow \chi_1 q \bar{q}'$ are always kinematically allowed for $\tau_{\chi_{2,3}} < 10^{12} \text{ s}$. The $\chi_{2,3}$ decays thus predominantly produce a small number of hadronic jets with a combined released hadronic energy $E_{\text{had}} \simeq E_{\text{vis}}$.

There are three distinct ranges of lifetimes [39]. For $0.1\text{ s} \lesssim \tau_{\chi_{2,3}} \lesssim 100\text{ s}$ the dominant effect is the inter-conversion between protons and neutrons, which overproduces the ^4He abundance. For longer lifetimes, $100\text{ s} \lesssim \tau_{\chi_{2,3}} \lesssim 10^7\text{ s}$, hadro-dissociation is the most efficient process and the bounds come from the non-thermal production of Li and D. At late times, $10^7\text{ s} \lesssim \tau_{\chi_{2,3}} \lesssim 10^{12}\text{ s}$, photo-dissociation caused by direct electromagnetic showers or by electromagnetic showers from daughter hadrons can lead to overproduction of ^3He .

We impose the ^4He , D and ^3He constraints¹ using the results in Ref. [39]. The visible energy release in the decays is $E_{\text{vis}} \sim \Delta m_{21,31}$. For $100\text{ GeV} < \Delta m_{21,31} < 10\text{ TeV}$ the constraints derived from the three relic mass benchmarks in Ref. [39] are well approximated by a power-law scaling with $E_{\text{vis}}^{-\eta_i}$. The exponents for the three constraints are $\eta_{^4\text{He}} \approx 1/3$, $\eta_{\text{D}} \approx 1/2$ and $\eta_{^3\text{He}} \approx 1$. For inter-conversion and hadro-dissociation the power-law scaling is expected to break down at energies below $\mathcal{O}(10)\text{ GeV}$ due to the presence of hadronic thresholds [39]. We thus do not extrapolate the fit results for ^4He and D for $\Delta m_{21,31}$ below 10 GeV . We assume that the photo-dissociation effects retain approximate power law behavior for E_{vis} large compared to the binding energies of the light nuclei, which is of the order of few tens of MeV. In our model for $\tau_{\chi_{2,3}} < 10^{2(12)}\text{ s}$, the mass splitting, $\Delta m_{21,31}$, is always above $10(0.1)\text{ GeV}$. Our approximations are thus always valid for ranges of lifetimes for which the ^3He constraints are the most stringent. For the deuterium bound, on the other hand, the power-law scaling is expected to fail for part of the parameter space where the bound is the most stringent, since $\Delta m_{21,31}$ can be as low as a few GeV. We have checked using the power-law derived bound that these regions are excluded by several orders of magnitude. This gives us confidence to conclude that they remain excluded even with a more faithful treatment of hadro-dissociation effects.

In Fig. 5 we show the distribution of $\chi_{2,3}$ lifetimes in the viable parameter space of the fermionic DM model. The cosmological constraints rule out all points with $\tau_{2,3} \gtrsim 100\text{ s}$, which is the range of lifetimes for which the deuterium bound becomes effective. The points with lifetimes $\tau_{2,3} \lesssim 100\text{ s}$, on the other hand, are never excluded by cosmological constraints. This is the range of lifetimes where the most strigent bound comes from the ^4He abundance,

¹ The measured ^4He abundance has shifted upwards significantly since the publication of Ref. [39]. This should weaken the constraints for $\tau_{2,3} \lesssim 100\text{ s}$. The upward shift has no consequences for our conclusions since we find that the ^4He constraint from Ref. [39] is already never important in excluding the viable parameter space in our models.

which, however, is not sufficient to exclude any of our fermionic DM model points.

D. Direct and indirect dark matter searches

Both fermionic and scalar flavored DM can produce direct detection signal from DM scattering on nuclei. For fermionic DM the scattering is due to t -channel exchanges of FGBs. For scalar DM the scattering is dominated by the Higgs exchange in the t -channel, while the contribution of FGBs is in general negligible.

The spin-independent interactions with the nucleons for the fermionic flavored DM are described by the following effective Lagrangian [40, 41]

$$\mathcal{L}_{\text{dir.}} = f_p(\bar{\chi}\gamma_\mu\chi)(\bar{p}\gamma^\mu p) + f_n(\bar{\chi}\gamma_\mu\chi)(\bar{n}\gamma^\mu n). \quad (31)$$

The Wilson coefficients f_p and f_n are the couplings to protons and neutrons, respectively,

$$f_p = \sum_m (\hat{g}_\chi^m)_{11} \frac{2(\hat{\mathcal{G}}_V^u)_{11,m} + (\hat{\mathcal{G}}_V^d)_{11,m}}{m_{A^m}^2} \quad \text{and} \quad f_n = \sum_m (\hat{g}_\chi^m)_{11} \frac{(\hat{\mathcal{G}}_V^u)_{11,m} + 2(\hat{\mathcal{G}}_V^d)_{11,m}}{m_{A^m}^2}. \quad (32)$$

$\hat{\mathcal{G}}_V^{u,d}$ are the vectorial couplings of FGBs to quarks, defined in Eq. (25). The spin-independent DM–nucleon cross section as measured by the LUX experiment [42] is

$$\sigma_{\chi N}^{\text{SI}} = \left[1 + \frac{Z}{A} \left(\frac{f_p}{f_n} - 1 \right) \right]^2 \frac{\mu_{\chi n}^2 f_n^2}{\pi}, \quad (33)$$

where $\mu_{\chi n}$ is the reduced mass of the (χ, n) system. The Xenon atomic and mass numbers are denoted by Z and A , respectively. We thus have $Z = 54$, while A varies between 128 and 134. With the above relations we calculate the DM–nucleon cross section and compare it with the current best limits reported by the LUX experiment [42]. The results of the scan are shown in Fig. 8. Most of the points lie well below the present LUX bound. This is a consequence of the fact that the relic abundance is given by the s -channel resonant annihilation, while the direct detection scattering is due to t -channel exchanges of FGBs and thus not resonantly enhanced.

For scalar flavored DM the dominant scattering is through t -channel Higgs-boson exchange. This leads to the spin-independent scattering on nucleon $N = n, p$, [43, 44]

$$\sigma_{\chi N}^{\text{SI}} = \frac{\lambda_H^2 f_{N,h}^2}{4\pi} \left(\frac{m_{\phi_1} m_N}{m_{\phi_1} + m_N} \right)^2 \frac{m_N^2}{m_h^4 m_{\phi_1}^2}. \quad (34)$$

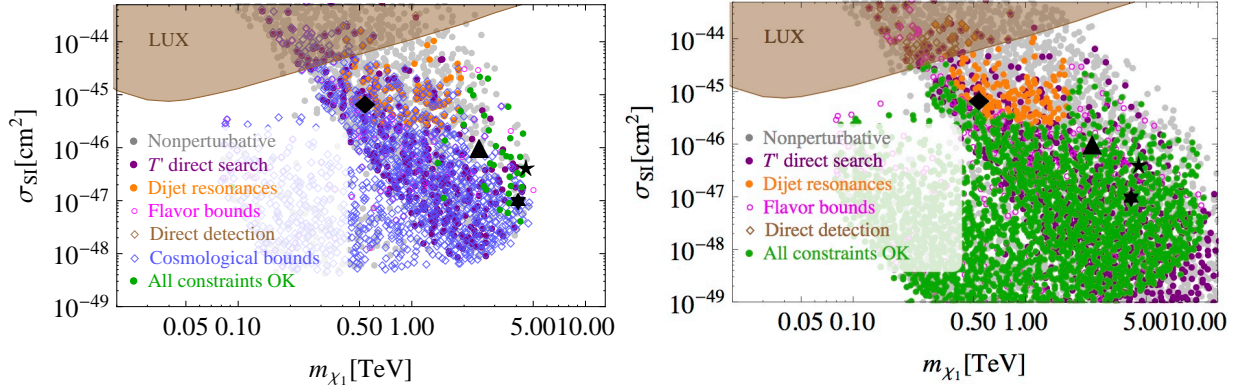


Figure 8: The predicted spin-independent cross section for DM scattering on nuclei as a function of DM mass for radiatively split fermionic DM (left) and in the large mass-splitting limit (right). The LUX bound is the brown shaded region. The color coding for the points is as in Fig. 3.

The Higgs–nucleon coupling is

$$f_{N,h} = \frac{2}{9} + \frac{7}{9} \sum_q f_q^{(N)}, \quad (35)$$

where the sum runs over the light quarks, $q = u, d, s$. $f_q^{(N)}$ are defined by the matrix elements of the light-quark scalar currents, $m_N f_q^{(N)} \equiv \langle N | m_q \bar{q}q | N \rangle$. For the s quark we use the lattice determination $f_s^{(N)} = 0.043 \pm 0.011$ [45]. The matrix elements for u and d quarks depend strongly on πN -scattering data. A Baryon Chiral Perturbation Theory (B χ PT) analysis of the πN -scattering data gives $\sigma_{\pi N} = 59(7)$ MeV [46]. This is in agreement with a B χ PT fit to world lattice $N_f = 2 + 1$ QCD data, which gives $\sigma_{\pi N} = 52(3)(8)$ MeV [47]. Including both $\Delta(1232)$ and finite-spacing parametrization in the fit shifts the central value to $\sigma_{\pi N} = 44$ MeV. To be conservative we use $\sigma_{\pi N} = (50 \pm 15)$ MeV that leads to $f_u^{(p)} = (1.8 \pm 0.5) \cdot 10^{-2}$, $f_d^{(p)} = (3.4 \pm 1.1) \cdot 10^{-2}$, $f_u^{(n)} = (1.6 \pm 0.5) \cdot 10^{-2}$, $f_d^{(n)} = (3.8 \pm 1.1) \cdot 10^{-2}$ by using expressions in Refs. [48, 49]. This results in $f_{N,h} = (29.7 \pm 1.3) \cdot 10^{-2}$ where we averaged over Higgs couplings to proton and neutron (the difference is an order of magnitude smaller than the quoted error). The resulting bound from the LUX experiment, assuming correct relic abundance, is shown in Fig. 7 and constrains $m_{\phi_1} \gtrsim 150$ GeV.

Finally, we discuss the constraints from indirect DM searches. The flavored DM annihilates to quarks so that the most constraining indirect DM searches are due to the photon and antiproton cosmic-ray fluxes. The constraints from the antiproton flux are quite depen-

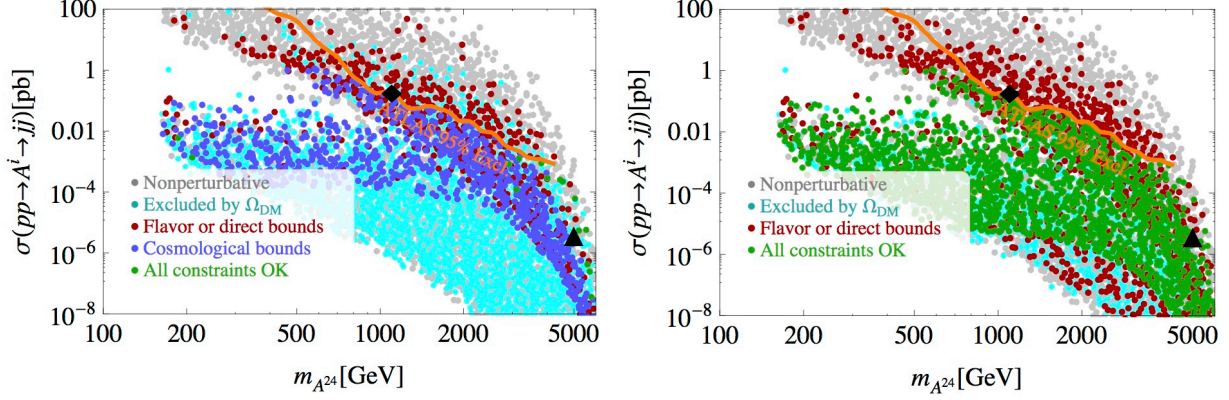


Figure 9: The dijet production cross section at 8 TeV LHC as a function of the lightest FGB mass for radiatively split fermionic DM (left) and in the large mass splitting limit (right). The 95% CL limit from Ref. [55] is denoted with a solid orange line. The color coding is the same as in Fig. 4.

dent on the propagation model. This can lead to almost an order of magnitude difference in uncertainty on the value of the excluded annihilation cross section [50].

For instance, by using the MED propagation model the antiproton-flux measurement by Pamela [51] constrains the DM mass to be $m_\chi \gtrsim 20$ GeV if the $\chi\chi^\dagger \rightarrow b\bar{b}$ annihilation dominates. Similar sensitivity is expected from annihilations to other quarks. The FERMI-LAT measurements of the photon flux from dwarf spheroidals bound $m_\chi \gtrsim 100$ GeV for thermal DM annihilating to quarks [52] (there are also slightly less stringent constraints from γ -ray emissions from the Large Magellanic Cloud [53], and from isotropic γ -ray background [54]).

E. Searches at the LHC

The searches for particles beyond the SM at the LHC are sensitive to the lightest new states in our models. The searches for dijet resonances impose constraints on the mass of the lightest FGB [55], and the searches for vector-like T and B quarks impose constraints on the mass of the lightest quark partners u'_i, d'_i [56].

The FGBs are narrow resonances that have flavor-conserving as well as flavor-violating couplings to the SM quarks, u_i, d_i , and to the quark partners, u'_i, d'_i . Since the FGBs are not colored they do not directly couple to gluons. At the partonic level the production process

is dominated by $q_i \bar{q}_j \rightarrow A^m \rightarrow q_k \bar{q}_l$. The FGBs would then appear as resonances in the dijet invariant-mass spectrum. For the most part, the LHC dijet resonance searches are relevant only for the lightest FGB which has, to a very good approximation, flavor-diagonal couplings to quarks. In this case, the cross section for $pp \rightarrow jj$ is given by [57, 58]

$$\sigma(pp \rightarrow q\bar{q}) = \sum_{i,j} \int_{4m_j^2}^s \frac{d\mathcal{M}^2}{s} \int_{-Y_B}^{Y_B} dy_B \int_{-z_o}^{z_o} dz f_i(\sqrt{\tau}e^{y_B}) f_{\bar{i}}(\sqrt{\tau}e^{-y_B}) \frac{1}{2} \frac{d}{dz} \hat{\sigma}_{ij}. \quad (36)$$

The partonic differential cross section is given by

$$\begin{aligned} \frac{d}{dz} \hat{\sigma}_{ij} = & \frac{1}{32\pi} \beta_f \frac{\mathcal{M}^2}{(\mathcal{M}^2 - m_{A^m}^2)^2 + m_{A^m}^2 \Gamma_{A^m}^2} \left(|\hat{\mathcal{G}}_V^{u,d}|_{ii,m}^2 + |\hat{\mathcal{G}}_A^{u,d}|_{ii,m}^2 \right) \\ & \times \left[\left(|\hat{\mathcal{G}}_V^{u,d}|_{jj,m}^2 + |\hat{\mathcal{G}}_A^{u,d}|_{jj,m}^2 \right) (1 + \beta_f^2 z^2) + 4 \left(|\hat{\mathcal{G}}_V^{u,d}|_{jj,m}^2 - |\hat{\mathcal{G}}_A^{u,d}|_{jj,m}^2 \right) \frac{m_j^2}{\mathcal{M}^2} \right], \end{aligned} \quad (37)$$

where, in the partonic center of mass frame, \mathcal{M} is the total energy, β_f is the velocity of the final-state quarks, $z = \cos \theta^*$ is the cosine of the polar angle of the outgoing quark w.r.t. the direction of the incoming quark, and the couplings $\hat{\mathcal{G}}_V$, $\hat{\mathcal{G}}_A$ of FGBs to quarks were defined in Eq. (25). We have only included the s -channel contribution that dominates on the FGB resonance peak. Terms odd in z were dropped in the differential cross section since they vanish after integration. The predicted dijet cross sections at the LHC with $\sqrt{s} = 8 \text{ TeV}$ are shown in Fig. 9, where the 95% CL exclusion from Ref. [55] is denoted with a solid orange line. This mostly excludes the points where the lightest FGB has large couplings to the quarks. Such points are in fact already mostly excluded either by the perturbativity requirement or from flavor constraints.

The quark partners, u'_i, d'_i , have an inverted mass hierarchy w.r.t. the SM quarks so that in most of our scan points the t' is the lightest state. The bound on the t' mass depends on the $t' \rightarrow bW$, $t'Z$, and $t'h$ branching ratios. The respective partial decay widths are given by

$$\Gamma(t' \rightarrow bW) = \frac{g_w^2}{64\pi} |s_{u_L3} V_{33} c_{d_L3}|^2 \frac{m_{t'}^3}{m_W^2} (1 - x_W^2)^2 (1 + 2x_W^2), \quad (38)$$

$$\begin{aligned} \Gamma(t' \rightarrow tZ) = & \frac{g_w^2}{128\pi} (c_{u_L3} s_{u_L3})^2 \frac{m_{t'}^3}{m_W^2} \sqrt{[1 - (x_Z + x_t)^2] [1 - (x_Z - x_t)^2]} \\ & \times [(1 - x_Z^2) (1 + 2x_Z^2 - x_t^2) - x_t^2 (1 - x_t^2)], \end{aligned} \quad (39)$$

$$\begin{aligned} \Gamma(t' \rightarrow th) = & \frac{\lambda_u^2}{64\pi} m_{t'} \sqrt{[1 - (x_h + x_t)^2] [1 - (x_h - x_t)^2]} \\ & \times [(s_{u_R3}^2 s_{u_L3}^2 + c_{u_R3}^2 c_{u_L3}^2) (1 + x_t^2 - x_h^2) - 4s_{u_R3} s_{u_L3} c_{u_R3} c_{u_L3} x_t], \end{aligned} \quad (40)$$

where $x_i = m_i/m_{t'}$ and s_i, c_i are the sines and cosines of the mixing angles between the SM and exotic quarks, while V is a unitary matrix describing the misalignment of the Y_u and Y_d vevs. Their definitions can be found in Ref. [23], where also the relevant Feynman rules are given. (We present the relevant Higgs Feynman rules in App. C, correcting an obvious typographical error of Ref. [23].) In Eq. (38) we took the limit $x_b \rightarrow 0$ that is justified since $m_{t'} \gg m_b$. We use the above expressions for the $t' \rightarrow bW, tZ, th$ branching ratios to obtain the 95% confidence-level bound on the t' mass by interpolating between quoted observed-limits table in [56].

F. Flavor constraints

The model of gauged-flavor symmetries in Eq. (6) was designed to be compatible with new TeV-scale dynamics and at the same time satisfy the tight flavor constraints from FCNC observables. The FCNCs induced by the exchange of new states are thus relatively mild. The light flavor-violating gauge bosons mediate $\Delta F = 2$ transitions at the tree-level, while the light exotic quarks modify the loop-induced SM process. These modifications are large enough that they restrict the parameter space of the model [23]. All the flavor-violating parameters in the model are fixed by requiring $\langle Y_u \rangle$ and $\langle Y_d \rangle$ to reproduce the observed masses and mixings in the quark sector. The size of the induced FCNCs thus depend only on a relatively small set of flavor conserving parameters in the model, the flavor symmetric masses and couplings. Following the analysis in Ref. [23] we focus on $\Delta F = 2$ observables in the neutral B and K sectors, and on $\bar{B}_s \rightarrow X_s \gamma$.

In our analysis we include the mass differences in the neutral K^0, B_s^0 , and B_d^0 sectors, $\Delta m_K, \Delta m_{B_d}$, and Δm_{B_s} , respectively. We also include the indirect CP violation in the kaon sector, ε_K , and the mixing-induced CP asymmetries $S_{\psi K_s}$ and $S_{\psi \phi}$. The corresponding mixing amplitude

$$2m_M (M_{12}^M)^* = \langle \bar{M} | \mathcal{H}_{\text{eff}}^{\Delta F=2} | M \rangle, \quad (41)$$

where $M = K^0, B_d^0, B_s^0$, controls all of these observables.

Two NP contributions to M_{12}^M dominate. These are the tree-level exchanges of FGBs and the loop-induced SM-like contribution with internal up-type quarks, including exotic quarks. For the later contribution we first integrate out at the EW scale, $\mu_W \simeq m_W$, the exotic quarks together with the W and the top quark. In this step we ignore the hierarchy of

masses between the exotic quarks and top. This is a good approximation for the dominant contribution that comes from t' . The theory matches onto the EFT with the SM effective weak operators. We perform the Renormalization Group (RG) of the Wilson coefficients to the low scale at which the hadronic matrix elements are evaluated on the lattice. For the tree-level FGB exchanges the hard scale is given by the corresponding gauge-boson masses. We integrate out the FGB at the corresponding hard scale and RG evolve the Wilson coefficients to the hadronic scale. The FGB exchanges generate four-fermion operators with the Dirac structures that differ from the SM one, namely $(\bar{f}_i \gamma_\mu P_R f_j)(\bar{f}_j \gamma^\mu P_R f_i)$ and $(\bar{f}_i \gamma_\mu P_R f_j)(\bar{f}_j \gamma^\mu P_L f_i)$, where i, j are the flavor indices. The RG evolution is implemented following Ref. [59] (for further details and the dependence of the numerical relevance with the scale see also Ref. [23]). For the non-perturbative inputs, the decay constants and the bag parameters, we use the current lattice averages [60].

The mass difference in the neutral kaon sector, Δm_K , and the CP-violating parameter ε_K are given by

$$\Delta M_K = 2 \operatorname{Re}(M_{12}^{K^0}), \quad \varepsilon_K = \frac{\kappa_\varepsilon e^{i\varphi_\varepsilon}}{\sqrt{2} \Delta M_K^{\text{exp}}} \operatorname{Im}(M_{12}^{K^0}), \quad (42)$$

with $\varphi_\varepsilon = (43.51 \pm 0.05)^\circ$ and $\kappa_\varepsilon = 0.923 \pm 0.006$, which includes long-distance effects in both $\operatorname{Im} M_{12}^{K^0}$ [61] and in the decay, i.e. $\operatorname{Im} \Gamma_{12}^{K^0}$ [62]. Our SM expectation for ε_K incorporates the known Next-to-Next-to-Leading-Order (NNLO) QCD corrections due to the charm [63] and charm-top [64] contributions.

The mass differences in the neutral B sectors are given by

$$\Delta M_{B_q} = 2|M_{12}^{B_q}|, \quad \text{with } q = d, s. \quad (43)$$

The CP violation in the neutral B sector is probed by the time-dependent asymmetries in the decays $B_d^0 \rightarrow \psi K_S$ and $B_s^0 \rightarrow \psi \phi$ that define the observables

$$S_{\psi K_S} = \sin(2\beta + 2\phi_{B_d}) \quad \text{and} \quad S_{\psi \phi} = \sin(2|\beta_s| + 2\phi_{B_s}), \quad (44)$$

respectively. In the conventional parametrization of the CKM matrix the SM phases are given by $V_{td}^{\text{SM}} = |V_{td}^{\text{SM}}|e^{-i\beta}$ and $V_{ts}^{\text{SM}} = -|V_{ts}^{\text{SM}}|e^{-i\beta_s}$. The NP phases are defined through the relation $M_{12}^{B_q} = |M_{12}^{B_q}| e^{2i(\beta_q + \phi_{B_q})}$. The tree level exchanges of FGBs induce such new phases in $\Delta F = 2$ matrix elements. These are thus constrained both by the $S_{\psi K_S}$ and $S_{\psi \phi}$ asymmetries, and by ε_K in the kaon sector.

The rate of $\bar{B} \rightarrow X_s \gamma$ is also modified by the presence of exotic up-type quarks. These can only enhance the $\bar{B} \rightarrow X_s \gamma$ rate with respect to the SM expectations [9]. The contributions of FGBs are loop-suppressed. Even though they may be enhanced by $m_{b'}$ they are negligible in models with a seesaw-like mass generation for quarks, like the model we consider [65]. The SM prediction for the rate in our analysis includes the known NNLO corrections [66–68].

In our numerical scan we mark parameter space points to have passed the flavor constraints only if the predictions for all our observables lie within three standard deviations of the corresponding experimental values. Whenever theoretical uncertainties are relevant, we include them in quadrature with the experimental ones.

The deviations of the selected FCNC observables from the SM predictions for the four benchmark points are shown in Figs. 10 to 12.

V. BENCHMARKS

To illustrate the most relevant phenomenology of fermionic flavored DM we select four representative benchmark points. The main features of the four benchmarks are summarized in Figs. 10–13. The upper panels in the figures show the spectra for the FGBs, A^m , the quark partners, u'_i, d'_i , and the DM multiplet, χ_i . Each FGB is represented by four shaded 3×3 rasters. The shade of the entries in the rasters is approximately logarithmically proportional to the size of the couplings to u_R, d_R, u_L and d_L , respectively (from left to right). The DM relic abundances as functions of the χ_1 mass are shown in the bottom left panels. The lines correspond to our approximate calculation for a radiatively split DM multiplet (red solid line) and for a DM multiplet with large mass splittings (black dashed line). The open diamonds (circles) correspond to the solutions of the coupled Boltzmann equations for the radiative (large) splitting cases which were calculated in **MadDM**. The approximate and **MadDM** relic-abundance calculations are in very good agreement for this small subset of benchmarks. In general, however, a disagreement of up $\mathcal{O}(30\%)$ could be expected due to the approximations (see App. B for a more detailed discussion). The bottom right panels show the pull in selected flavor observables, i.e., the differences between theoretical predictions and measurements normalized to the $1\text{-}\sigma$ uncertainties. The uncertainties were obtained by adding in quadrature the theory and experimental errors. The four benchmark points are also marked in Figs. 3, 4, and 5 with a diamond (1), a five-point star (2), a triangle (3), and

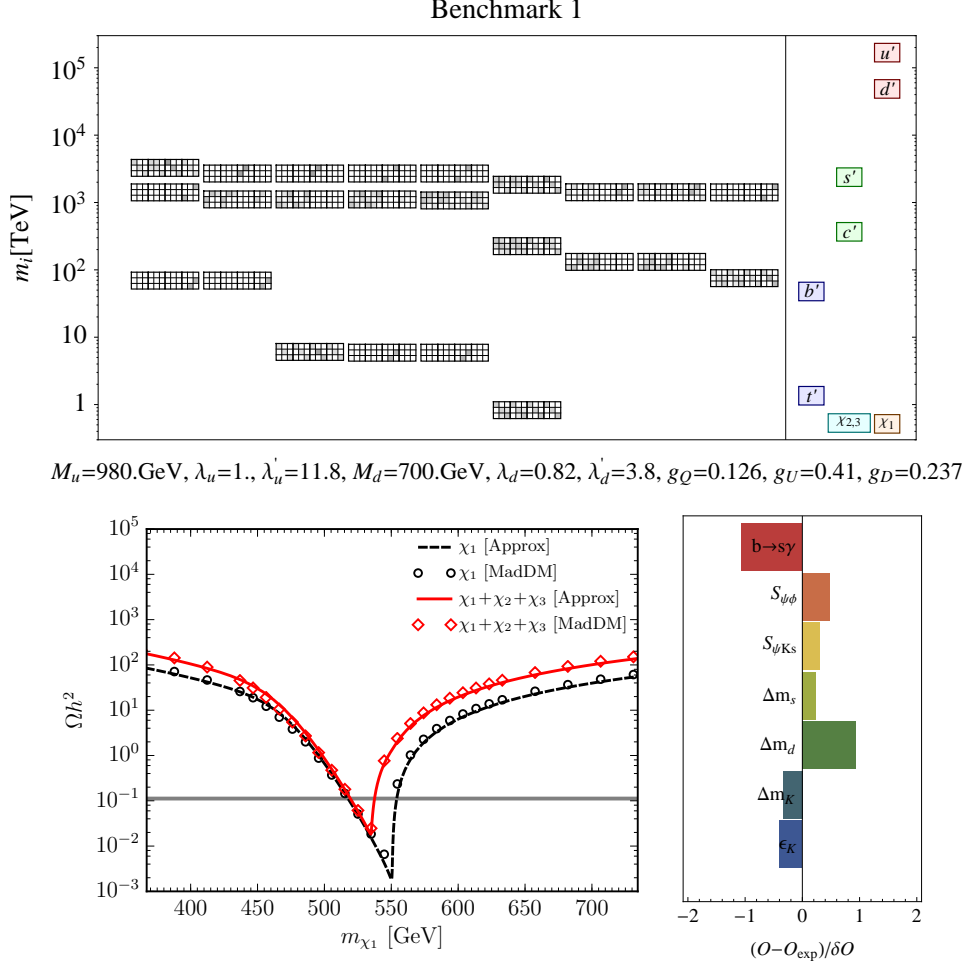


Figure 10: Mass spectrum and flavor decomposition (upper panel), DM relic density as a function of the DM mass with all other parameters fixed (lower left panel) and the pattern of effects in selected flavor observables (lower right panel) for the fermionic flavored DM benchmark 1. The input benchmark-point parameters are listed in the center. See text for details.

a six-point star (4).

“*Benchmark 1*” is an example of fermionic flavored DM, where the DM multiplet is light, with mass below 1 TeV. The mass of the lightest state in the DM multiplet is $m_{\chi_1} \simeq 520(540)$ GeV if it lies just below (above) the LFGB resonance. If the mass splitting between χ_1 , χ_2 and χ_3 is solely due to radiative corrections, χ_2 and χ_3 are almost mass degenerate with masses roughly 10 GeV above m_{χ_1} , and χ_3 is about 100 MeV heavier than χ_2 . The lightest quark partner is t' with a mass $m_{t'} \simeq 1.3$ TeV. The lightest FGB has a mass $m_{A^{24}} \simeq 1.1$ TeV. All the remaining NP states are above 7 TeV. This benchmark point demonstrates that even

parameter regions with low lying FGBs can be consistent with both the resonance searches and the FCNC bounds. The most robust constraints in this parameter region come from cosmology (in case of radiatively-split DM masses) and dijet-resonance searches (see Figs. 5 and 9). Note in particular that for the completely (mass) decoupled fermionic DM scenario, in which cosmology bounds are absent, all experimental constraints can be satisfied even for DM (and LFGB) masses below few 100 GeV.

The bottom left panel in Fig. 10 shows the predicted relic abundance for this benchmark, if only the DM mass is varied, which also modifies the splitting within the DM triplet. Relic abundance consistent with observations is obtained for a mass of DM close to half of the mass of the lightest FGB, in which case the annihilation cross section is resonantly enhanced. To saturate the observed DM relic density, two solutions for m_{χ_1} are obtained, with m_{χ_1} either above or below the resonant peak. We see that for radiatively split DM masses, where all χ_i components contribute to the DM relic density, m_{χ_i} need to lie within $\mathcal{O}(3\%)$ of the resonant peak for the annihilation to be strong enough. For completely decoupled DM multiplet the resonant condition is relaxed and needs to be satisfied to $\mathcal{O}(5\%)$.

In Fig. 10 (upper panel) we show the spectrum for the lower mass solution and radiative DM multiplet splitting. We see that the quark partners of the lighter generations are heavier than the partners of the third generation quarks. Similarly, the FGBs that couple more strongly to the first two generations are typically heavier than the ones that couple preferably to the third generation. The couplings of the lightest FGB to the light quarks have the form $\hat{\mathcal{G}}_L^u \simeq \hat{\mathcal{G}}_R^u \simeq \hat{\mathcal{G}}_L^d \simeq \hat{\mathcal{G}}_R^d \propto \lambda^8$, where the relative corrections to this relation are below the percent level. This means that the lightest FGB couples to the light quarks vectorially, $\hat{\mathcal{G}}_A^{u,d} \ll \hat{\mathcal{G}}_V^{u,d}$, to a very good approximation. The same is true for the majority of parameter-space points passing flavor constraints.

The largest effects in flavor physics are in the mixing observables, the mass splittings $\Delta m_{d,s}$ in $B_d - \bar{B}_d$ and $B_s - \bar{B}_s$ systems, respectively, and the mass splitting in the $K - \bar{K}$ mixing, Δm_K , and the related CP violating parameter ϵ_K . The pulls in $b \rightarrow s\gamma$ and $B_d - \bar{B}_d$ mixing are due to the fact that the measurements agree with the SM prediction only at 1- σ level and the contribution to them from new states is very small.

“*Benchmark 2*” is an example of a generic parameter-space region, but towards the upper end of the perturbatively allowed region. The DM has a mass $m_{\chi_1} \simeq 4.5$ TeV, while the heavier states in the DM multiplet have masses 120 GeV and 150 GeV above m_{χ_1} (for the

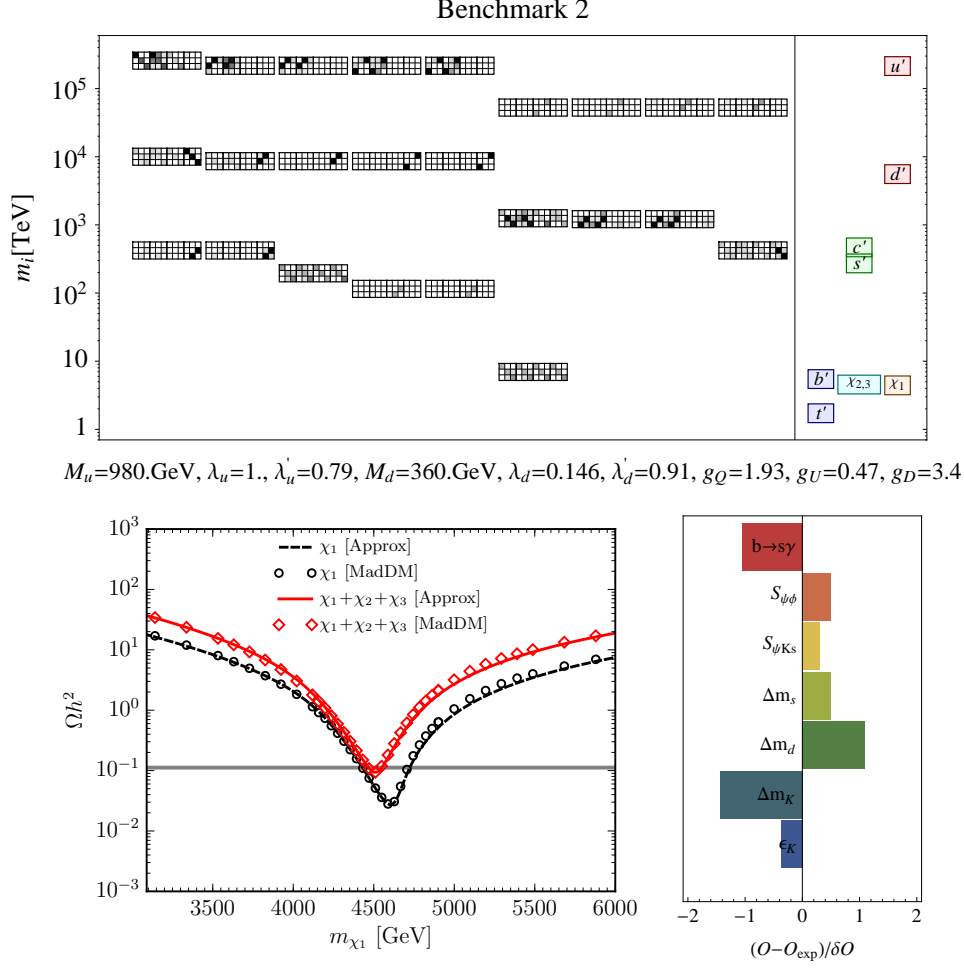


Figure 11: Same as Fig. 10 for benchmark 2.

case of only radiative mass splitting). The lightest exotic quark is the top partner with mass $m_{t'} \simeq 1.7 \text{ TeV}$, while the mass of the lightest FGB is $m_{A^{24}} \simeq 9.2 \text{ TeV}$.

For such high DM masses it is barely possible to obtain the correct relic abundance (see the lower left panel in Fig. 11). Therefore, the DM mass is finely tuned to be exactly on the resonant peak (see the lower left panel in Fig. 11), so $m_{\chi_i} \simeq m_{A^{24}}/2$. Because of the high masses of the NP states the direct searches (direct DM detection, t' searches and dijet resonance searches) as well as the indirect flavor constraints are easily avoided, although $K - \bar{K}$ mixing does receive non-negligible contributions.

Also in this case, the couplings of the lightest FGB to the light quarks have the form $\hat{\mathcal{G}}_L^u \simeq \hat{\mathcal{G}}_R^u \simeq \hat{\mathcal{G}}_L^d \simeq \hat{\mathcal{G}}_R^d \propto \lambda^8$, so the couplings of the lightest FGB to quarks are to a good extent vectorial.

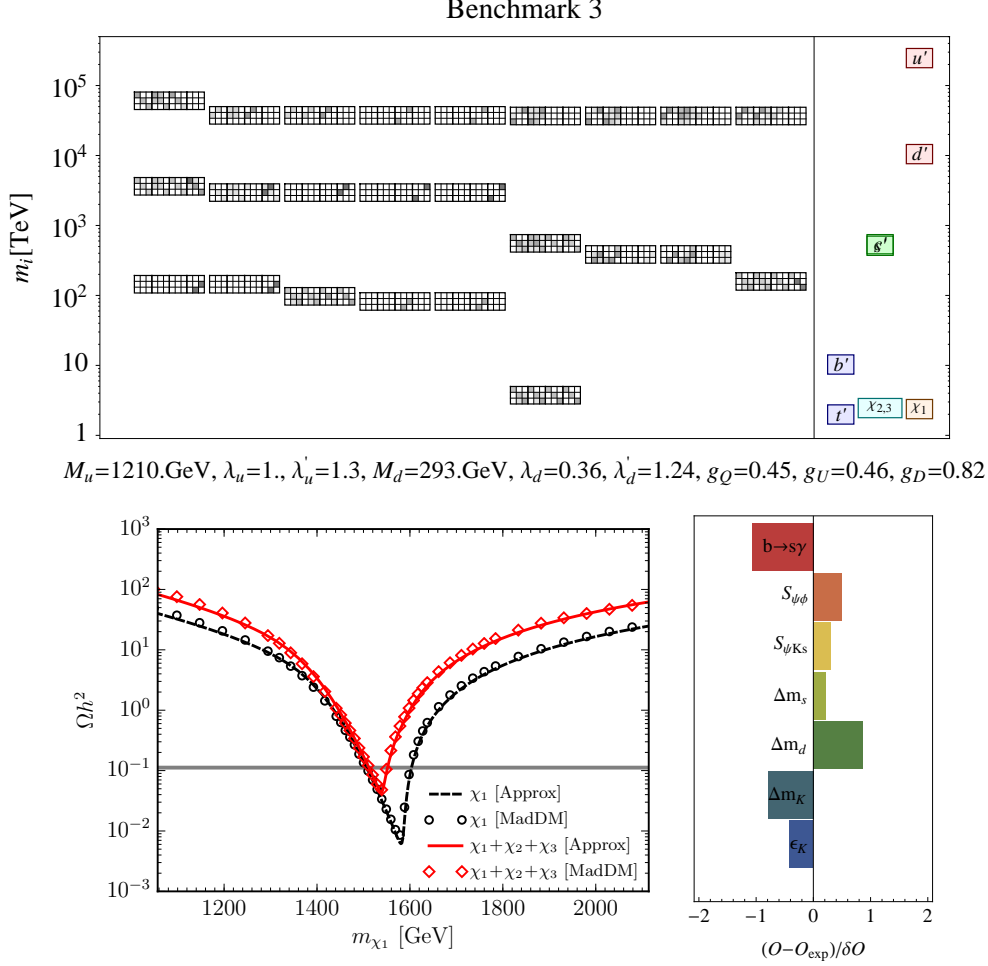


Figure 12: Same as Fig. 10 for benchmark 3.

“*Benchmark 3*” is an example of a generic parameter space in which all the couplings of the model are well below the perturbativity bounds. The lightest FGB has a mass $m_{A^{24}} \simeq 5$ TeV while all other FGBs have masses above 100 TeV. The lightest partner quark is t' with mass $m_{t'} \simeq 2$ TeV. The DM states have masses $m_{\chi_1} \simeq 2.4$ TeV and $m_{\chi_2} \simeq m_{\chi_3} = 2.5$ TeV (for radiative mass splitting). All direct experimental constraints as well indirect flavor bounds are easily satisfied in this case. For radiatively DM mass splitting the cosmological constraints are the most constraining. In particular, requiring small enough $\tau_{\chi_{2,3}}$ (or equivalently large enough $\Delta m_{21,31}$) typically imposes a lower bound on g_U .

“*Benchmark 4*” is an example of the case in which the next-to-lightest FGBs have masses not too far from the lightest FGB. In the benchmark point the lightest FGB has a mass $m_{A^{24}} \simeq 8.3$ TeV, while the next to lightest FGBs have masses $m_{A^{23}} \simeq m_{A^{22}} \simeq 19$ TeV,

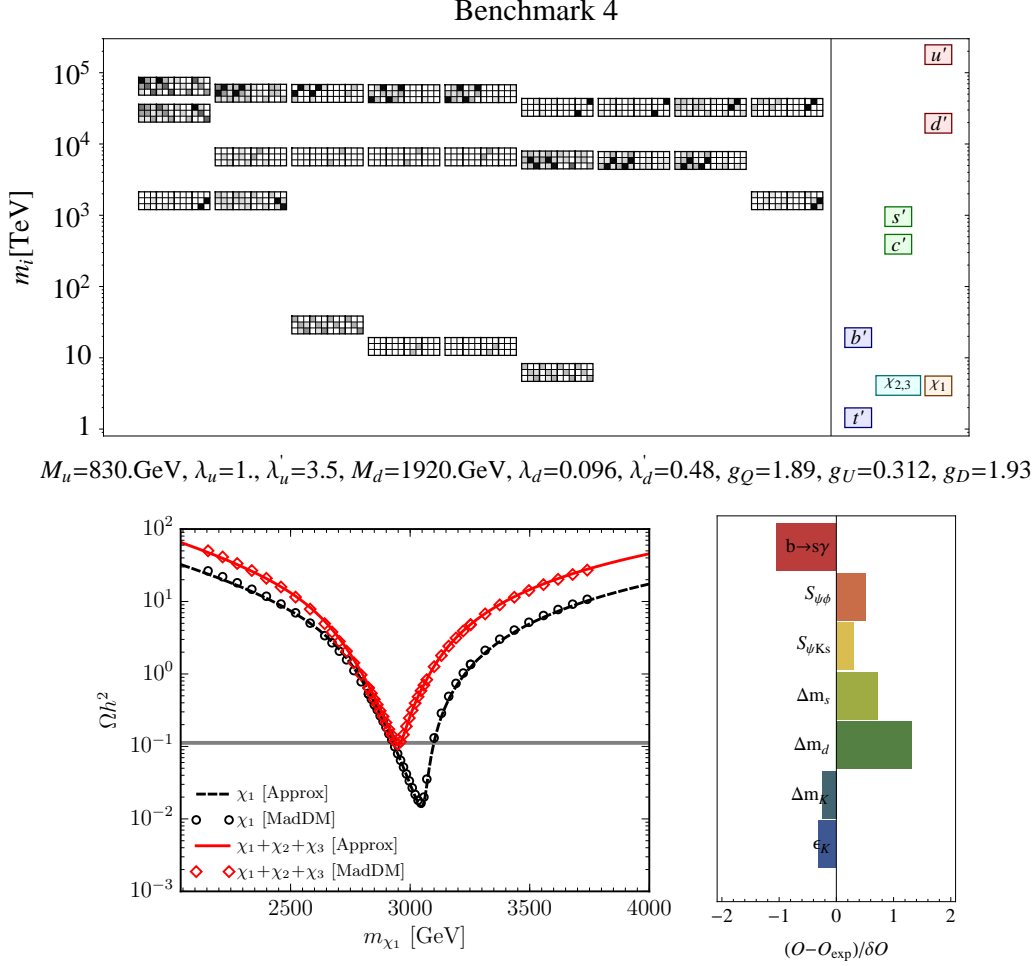


Figure 13: Same as Fig. 10 for benchmark 4.

$m_{A^{21}} \simeq 39 \text{ TeV}$. In this case the deviations from the $\hat{\mathcal{G}}_L^u \simeq \hat{\mathcal{G}}_R^u \simeq \hat{\mathcal{G}}_L^d \simeq \hat{\mathcal{G}}_R^d \propto \lambda^8$ relation for the lightest FGB coupling to quarks are of $\mathcal{O}(10\%)$. Nonetheless, this does not have a significant effect on the computation of the DM relic abundance. This is demonstrated in Fig. 13 bottom left panel where a comparison is shown between the relic-abundance calculation neglecting (dashed lines, labelled “Approx”) and including (full lines, using MadDM) flavor off-diagonal lightest FGB couplings and contributions of heavier FGBs. For a more detailed discussion of these effects see Appendix B.

The lightest quark partner is t' with mass $m_{t'} \simeq 1.4 \text{ TeV}$, and is significantly lighter than all FGBs and also DM. The DM states are degenerate to a good approximation, with masses $m_{\chi_1} = 4.1 \text{ TeV}$ and $m_{\chi_2} \simeq m_{\chi_3} \simeq 4.2 \text{ TeV}$. Because of the light t' the flavor constraints are nontrivial, and there are visible effects in B_d and B_s mixing observables.

VI. CONCLUSIONS

We investigated the possibility that DM is in a nontrivial representation of the continuous flavor group $\mathcal{G}_F^{\text{SM}} = SU(3)_Q \times SU(3)_U \times SU(3)_D$. The two main results are that (i) one can have a viable model of DM where DM is stable because it is charged under \mathcal{Z}_3^X – a discrete central subgroup of $\mathcal{G}_F^{\text{SM}}$ and color $SU(3)$, and (ii) that the DM spectrum can be very non-MFV like, while all the low-energy constraints will appear MFV-like.

\mathcal{Z}_3^X is exactly conserved in many models of flavor. For instance, it remains unbroken for MFV new physics. More generally, \mathcal{Z}_3^X remains exact if the flavor group $\mathcal{G}_F^{\text{SM}}$ is broken only by the vevs of scalar fields, or condensates, with zero flavor triality. Examples of zero flavor triality fields are scalars in bifundamental or in adjoint representations of the flavor $SU(3)$'s. The basic requirement for this set-up is that $\mathcal{G}_F^{\text{SM}}$ is a good symmetry in the UV. This is achieved, if $\mathcal{G}_F^{\text{SM}}$ is fully gauged in the UV, which is the possibility we explored. The DM is then stable because it is \mathcal{Z}_3^X odd, while all SM fields are \mathcal{Z}_3^X even.

We investigated two different types of flavored DM models: (i) models in which the leading interaction of the DM with the visible sector is through the flavored gauge bosons (FGBs), and (ii) models in which the contributions from the FGB exchanges are subleading.

As an example of the first type of models we considered a Dirac fermion DM that is in a fundamental representation of $SU(3)_U$. The relic abundance is fixed by the resonant DM annihilation to SM particles through the s -channel exchange of the lightest FGB. The DM is thus required to have a mass of about half of the lightest FGB's mass. This in turn implies that the FGBs cannot be arbitrarily heavy, but at most $\mathcal{O}(10 \text{ TeV})$. Such light FGBs are possible, if the masses of FGBs are inversely proportional to the corresponding quark masses. That is, if the FGBs that couple most strongly to light quarks are also the heaviest. To achieve this we adopted the model of Ref. [9] in which the inverse proportionality is achieved by introducing a set of quark partners also necessary to cancel gauge anomalies. The same quark partners also mix with the SM quarks and lead to the mass hierarchy of the SM quark masses.

The flavor and collider phenomenology of the model is very similar to the case where DM is not considered. The fact that the first-generation quark partners are the heaviest and that the spectrum is completely split, signals the non-MFV character of the model. However, the low-energy consequences are MFV-like (see Appendix A). The flavor constraints are

satisfied even with FGBs and the top-quark partner, with masses potentially well below the TeV scale. The relevant direct collider searches are the searches for dijet resonances and t' searches. They exclude part of the available parameter space. Requiring that there is a thermal relic DM introduces new constraints. Because DM is part of a flavor multiplet the heavier DM states need to decay before big bang nucleosynthesis. In the case of radiatively-split fermionic DM this excludes a large part of the parameter space. The remaining points are mostly safe from direct-detection bounds. The fact that the DM mass is related to the FGB mass by the requirement of almost resonant annihilation sets both lower and upper bounds on the DM mass. Requiring that the theory is perturbative also puts an upper bound on the DM mass, $m_{\chi_1} \lesssim 5 \text{ TeV}$. On the other hand, requiring that the FGBs satisfy flavor and direct constraints and that DM is simultaneously in accordance with cosmological constraints leads to a lower bound on the DM mass, $m_{\chi_1} \gtrsim 500 \text{ GeV}$. Improved bounds on dijet resonances at the LHC are expected to further strengthen this constraint (see Fig. 9).

We have also considered the possibility that the DM multiplet is split due to an extra source of flavor breaking. Also in this case, the correct relic abundance requires resonant annihilation. The DM mass is in thus still roughly equal to half of the mass of the lightest FGB. However, the heavier DM states decay well before big bang nucleosynthesis so that a much wider range of DM masses is phenomenologically viable. In our scan this includes DM masses as light as 100 GeV (with very small couplings to FGBs) and up to 10 TeV .

A possible signal of the gauged flavor model with fermionic DM at the LHC are mono-jets, where the lightest FGB is produced associated with initial state radiation and decays to χ_1 pairs. The χ_1 s are expected to be non-relativistic in the lightest FGB's rest frame, as their combined mass needs to be close to the FGB mass to fulfill the resonance condition for relic DM abundance. In the event that such a signal would eventually emerge, the corresponding dijet-resonance signal is generically also expected in the model. A final possibility in the case of radiatively split DM mass spectrum is that some of the lightest FGBs decay to slow-moving $\chi_{2,3}$. They in turn decay within the detector, leaving (highly) displaced vertices, isolated hits in the calorimeter or in the muon chambers. Unfortunately, in most of the parameter space $\chi_{2,3}$ are expected to decay well outside the detectors, see Fig. 5, leaving mono-jets as the only signal.

In the second type of models, where FGB exchanges give only subleading contributions, the only visible consequence of the flavor dynamics on the DM is that DM is stable. The

DM mass and the mass of the lightest FGB are no longer connected. We show this in the example of scalar flavored DM, in which the dominant interactions with the visible sector are through the Higgs portal operator. In this case the phenomenology of the DM is to a very good approximation the same as in the Higgs-portal scalar DM, while the dynamics of FGBs and quark partners is unrelated to DM.

In short, we have shown, using an explicit renormalizable model, that it is possible for flavored DM to be a thermal relic. The considered model is not the only choice. One could consider DM in other representations of $\mathcal{G}_F^{\text{SM}}$. Our analysis can be extended also in other ways: for instance, by enlarging the global symmetry as in Ref. [13] and subsequently gauging it. For instance, with our field content the global group is $\mathcal{G}_F^{\text{SM}} \times SU(3)_\chi$, where χ is in the fundamental of $SU(3)_\chi$. In our work we have identified $SU(3)_\chi$ with $SU(3)_U$, but other choices could be made. Yet another possibility is to gauge only part of $\mathcal{G}_F^{\text{SM}}$, for instance a $U(2)^3 \subset \mathcal{G}_F^{\text{SM}}$. Note that for fermionic DM, \mathcal{Z}_3 is part of an accidental $U(1)_\chi$ acting in the dark sector. The $U(1)_\chi$ can be broken by the dimension-7 operator $LH\chi\chi\chi$, but is exact in our renormalizable model. It can in principle be gauged and lead to additional phenomenology. If DM is a scalar, $U(1)_\chi$ can be broken already at the renormalizable level, leaving only \mathcal{Z}_3 exact.

Acknowledgements. We thank Csaba Csaki, Gino Isidori, Graham Kribs and Christopher Smith for enlightening discussions. J.Z. and F.B. are supported by the U.S. National Science Foundation under CAREER Grant PHY-1151392. This work was supported in part by the Slovenian Research Agency. F.B. is grateful for the hospitality of the Fermilab theory department. Fermilab is operated by Fermi Research Alliance, LLC under Contract No. DE-AC02-07CH11359 with the United States Department of Energy. The work of DR is supported by the NSF under grant No. PHY-1002399.

Appendix A: Minimal flavor violation with gauged flavor symmetries

In this appendix we verify numerically that the Wilson coefficients in the weak Hamiltonian for B_d and B_s mixing,

$$\mathcal{H}_{\text{eff}}^{\Delta B=2} = \sum_{i=1}^5 C_i^{bq} Q_i^{bq} + \sum_{i=1}^5 \tilde{C}_i^{bq} \tilde{Q}_i^{bq}, \quad (\text{A1})$$

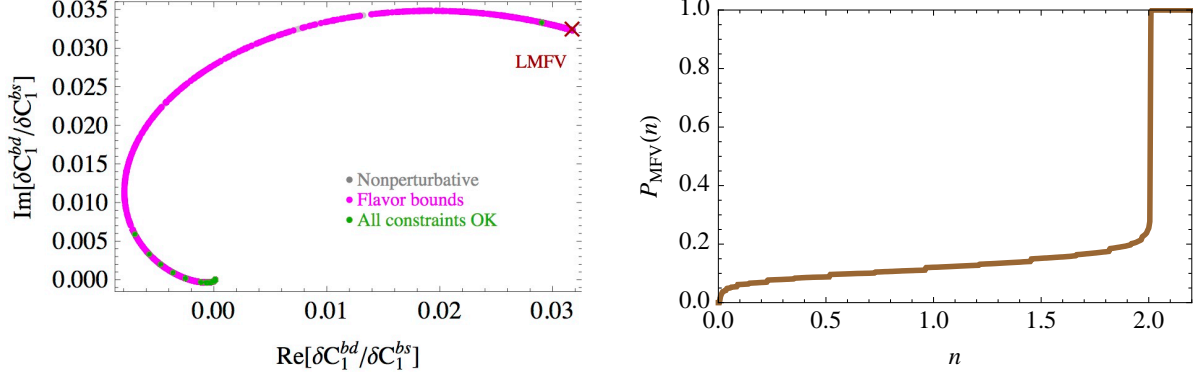


Figure 14: The FGB contributions to the $V-A$ current operator in the effective weak Hamiltonian. The left panel shows the values of the complex ratio $\delta C_1^{bd}/\delta C_1^{bs}$ for our scan points, with green points satisfying all constraints, magenta points excluded by flavor constraints and grey points by perturbativity considerations. The cross denotes the point $\delta C_1^{bd}/\delta C_1^{bs} = (V_{td}^*/V_{ts}^*)^2$. In this point the MFV operator with the smallest number of Yukawa insertions completely dominates. The right panel shows the cumulative function $P_{\text{MFV}}(n)$, see Eq. (A4).

generated from exchanges of flavored gauge bosons, are of the MFV type. A tree-level exchange of FGBs generates contributions to B_d mixing through operators

$$Q_1^{bd} = \bar{d}_L^\alpha \gamma_\mu b_L^\alpha \bar{d}_L^\beta \gamma_\mu b_L^\beta, \quad Q_3^{bd} = \bar{d}_R^\alpha b_L^\beta \bar{d}_R^\beta b_L^\alpha, \quad (\text{A2})$$

and $\tilde{Q}_1^{bd}, \tilde{Q}_3^{bd}$, that follow from Q_1^{bd}, Q_3^{bd} with $P_L \leftrightarrow P_R$ exchange (the remaining operators can be found in, e.g., Ref. [69]). If the lightest FGB has predominantly left-handed couplings, then the C_1^{bd} Wilson coefficient is the largest one. If the lightest FGB couples predominantly to the right-handed quarks, then \tilde{C}_1^{bd} dominates. For comparable left- and right-handed couplings all four Wilson coefficients, $C_{1,3}^{bd}, \tilde{C}_{1,3}^{bd}$, are important. The analogous discussion applies to the case of FGB contributions to B_s mixing obtained with a trivial $d \rightarrow s$ exchange.

As discussed in Section III the contributions from the gauged flavor model is expandable in terms of the SM Yukawas. The contributions due to FGB exchanges can thus be written as

$$\delta C_1^{bd} = c_1 (y_u y_u^\dagger)_{13}^2 + c_2 (y_u y_u^\dagger)_{13} (y_d y_d^\dagger y_u y_u^\dagger)_{13} + \dots = c_1 (V_{td}^* V_{tb})^2 + c_2 y_d^2 (V_{td}^* V_{tb})^2 + \dots, \quad (\text{A3})$$

where $(y_d)_{ij} = \text{diag}(y_d, y_s, y_b)$, and we set $y_t = 1$ in the second equality. In Eq. (A3) we kept only the two terms relevant for the discussion below. The same expansion applies for δC_1^{bs} with the replacement $d \rightarrow s$ in Eq. (A3).

In Fig. 14 (left) we show the ratio $\delta C_1^{bd}/\delta C_1^{bs}$, i.e. the NP contribution to the $V - A$ quark current operator due to tree-level FGB exchanges. Note that the ratio $\delta C_1^{bd}/\delta C_1^{bs}$ can be complex. If c_1 , i.e. the leading MFV (LMFV) term, dominates then $\delta C_1^{bd}/\delta C_1^{bs} \simeq (V_{td}^*/V_{ts}^*)^2$. This is denoted by a cross in Fig. 14 (left). The addition of the operators with extra insertions of $y_d y_d^\dagger$ leads to $\delta C_1^{bd}/\delta C_1^{bs}$ not being equal to $(V_{td}^*/V_{ts}^*)^2$. We verified that the curve for $\delta C_1^{bd}/\delta C_1^{bs}$ shown in Fig. 14 (left) can be fitted with the form of $\delta C_1^{bd,bs}$ in Eq. (A3) by taking c_1 real, c_2 complex, and varying c_1 from $\mathcal{O}(1)$ to vanishingly small. The points in our scan can be grouped into two sets. For the first set of points both c_1 and c_2 terms are sizeable. For the second set of points the c_1 term is negligible and c_2 dominates. This is shown in Fig. 14 (right), where we plot the cumulative distribution function

$$P_{\text{MFV}}(n) = \frac{N(|\delta C_1^{bd}/\delta C_1^{bs}| \geq (m_d/m_s)^n |V_{td}^*/V_{ts}^*|^2)}{N_{\text{total}}}. \quad (\text{A4})$$

The function $P_{\text{MFV}}(n)$ can be interpreted as the fraction of points that have the ratio $|\delta C_1^{bd}/\delta C_1^{bs}|$ effectively dominated by operators with up to y_d^n insertions. That is, the points dominated by the c_1 term contribute to $P_{\text{MFV}}(0)$ (and to $P_{\text{MFV}}(n)$ with $n \geq 0$), while the points dominated by the c_2 term contribute to $P_{\text{MFV}}(2)$ (and to $P_{\text{MFV}}(n)$ with $n \geq 2$). The points with both c_1 and c_2 start contributing to $P_{\text{MFV}}(n)$ for n somewhere between 0 and 2, depending on the relative sizes of c_1 and c_2 . Fig. 14 (right) shows that the c_1 term dominates in a subleading (but nonzero) set of points, that about 10% points have both sizeable c_1 and c_2 terms, and that c_2 dominates in about 80% of the points.

The similar analysis can be performed for $V + A$ operators, \tilde{Q}_1^{bd} and \tilde{Q}_1^{bs} . We expand the FGB contributions to their respective Wilson coefficients in terms of the SM Yukawas

$$\begin{aligned} \delta \tilde{C}_1^{bd} &= \tilde{c}_1 (y_d^\dagger y_u y_u^\dagger y_b)_{13}^2 + \tilde{c}_2 (y_d^\dagger y_u y_u^\dagger y_b)_{13} (y_d^\dagger y_d y_d^\dagger y_u y_u^\dagger y_b)_{13} + \dots \\ &= \tilde{c}_1 y_d^2 y_b^2 (V_{td}^* V_{tb})^2 + \tilde{c}_2 y_d^4 y_b^2 (V_{td}^* V_{tb})^2 + \dots, \end{aligned} \quad (\text{A5})$$

and similarly for $\delta \tilde{C}_1^{bs}$ with the $d \rightarrow s$ replacement. We show in Fig. 15 (left) the ratio $\tilde{C}_1^{bd}/\tilde{C}_1^{bs}$ for our scan. If the \tilde{c}_1 term dominates, then $\tilde{C}_1^{bd}/\tilde{C}_1^{bs} = (m_d/m_s)^2 (V_{td}^*/V_{ts}^*)^2$, which is denoted by the cross in Fig. 15 (left). The points for which also the \tilde{c}_2 operator (and other operators denoted by ellipses above) is important then lie away from the $\tilde{C}_1^{bd}/\tilde{C}_1^{bs} = (m_d/m_s)^2 (V_{td}^*/V_{ts}^*)^2$ region. We also define a cumulative function

$$\tilde{P}_{\text{MFV}}(n) = \frac{N(|\delta \tilde{C}_1^{bd}/\delta \tilde{C}_1^{bs}| \geq (m_d/m_s)^{n+2} |V_{td}^*/V_{ts}^*|^2)}{N_{\text{total}}}. \quad (\text{A6})$$

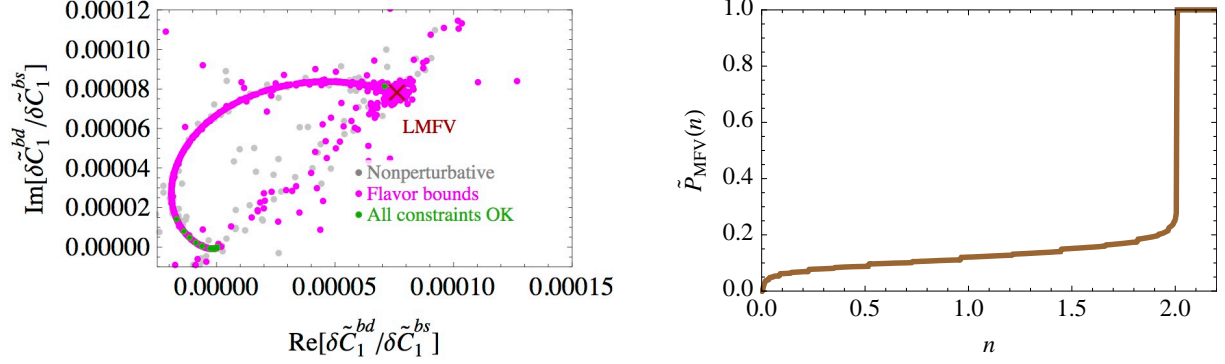


Figure 15: The FGB contributions to $V + A$ current operator in the effective weak Hamiltonian. Left panel shows the complex ratio $\delta\tilde{C}_1^{bd}/\delta\tilde{C}_1^{bs}$ for our scan points with the same color coding as in Fig. 14. The cross denotes the point $\delta\tilde{C}_1^{bd}/\delta\tilde{C}_1^{bs} = (m_d/m_s)^2(V_{td}^*/V_{ts}^*)^2$, obtained if the MFV operator with the smallest number of Yukawa insertions dominates. The right panel shows the cumulative function $\tilde{P}_{\text{MFV}}(n)$, see Eq. (A6).

The values for $\tilde{P}_{\text{MFV}}(n)$ are shown in Fig. 15 (right). We see that also in this case the points cluster into two groups, with vanishing \tilde{c}_1 term or with both \tilde{c}_1 and \tilde{c}_2 relevant.

The above analysis demonstrates that the FGB contributions to the Wilson coefficients in the effective weak Hamiltonian can be expanded in terms of the SM Yukawas. This is a hallmark of (general) MFV. In particular, the expansion in terms of $m_{d,s}/m_b$ and off-diagonal CKM elements can still be performed and is not ruined by the large ratios of scales present in the problem such as the very disparate FGB masses.

Appendix B: Thermal relic computation

In this appendix we describe the calculation of relic density that was used in the scans in the main part of the paper. Several approximations to the coupled Boltzmann equations were necessary in order to reduce the evaluation time per benchmark and thus allow adequate coverage of the parameter space. We find the approximate solutions to be in agreement with the full solutions at the $\mathcal{O}(30\%)$ level. The full numerical solution of the Boltzmann equations was obtained with **MadDM** [27] using a **UFO** model file [70], which was generated with the **FeynRules** package [28].

Denoting the DM multiplet by φ , where φ is either a Dirac fermion or a complex scalar,

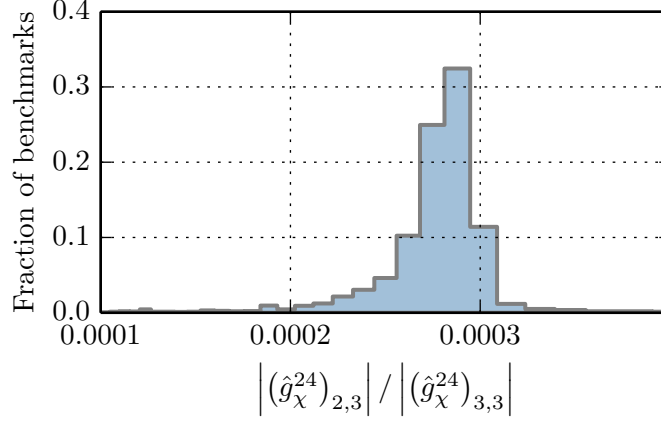


Figure 16: The fraction of benchmarks as a function of the off-diagonal couplings of the heaviest and next-to-heaviest DM components to the lightest FGB (A^{24}) normalized by the diagonal coupling of the heaviest component.

the most general set of coupled Boltzmann equations reads [25]

$$\begin{aligned}
\frac{dn_{\varphi_i}}{dt} + 3Hn_{\varphi_i} = & - \sum_j \langle \sigma(\varphi_i \varphi_j \leftrightarrow XX) v_{\text{lab}} \rangle \left(n_{\varphi_i} n_{\varphi_j} - n_{\varphi_i}^{\text{EQ}} n_{\varphi_j}^{\text{EQ}} \right) \\
& - \sum_{j \neq i} \langle \sigma(\varphi_i X \leftrightarrow \varphi_j X) v_{\text{lab}} \rangle \left(n_{\varphi_i} - \frac{n_{\varphi_i}^{\text{EQ}}}{n_{\varphi_j}^{\text{EQ}}} n_{\varphi_j} \right) n_X^{\text{EQ}} \\
& - \sum_{j \neq i} \langle \sigma(\varphi_i \varphi_j \leftrightarrow \varphi_k \varphi_\ell) v_{\text{lab}} \rangle \left(n_{\varphi_i} n_{\varphi_j} - \frac{n_{\varphi_i}^{\text{EQ}} n_{\varphi_j}^{\text{EQ}}}{n_{\varphi_k}^{\text{EQ}} n_{\varphi_\ell}^{\text{EQ}}} n_{\varphi_k} n_{\varphi_\ell} \right) \\
& \pm \sum_{j \neq i} \left[\langle \Gamma(\varphi_{j,i} \rightarrow \varphi_{i,j} X) \rangle n_{\varphi_{j,i}} + \langle \sigma(\varphi_{j,i} X \rightarrow \varphi_{i,j}) \rangle n_{\varphi_{j,i}} n_X^{\text{EQ}} \right],
\end{aligned} \tag{B1}$$

where X denotes a generic SM state. For large mass splittings between the φ components it is sufficient to consider the lightest φ_i state in Eq. (B1). The contributions to the DM relic density from the heavy φ components are exponentially suppressed by corresponding Boltzmann factors and can be neglected within our precision. In contrast, when the mass splittings are small the full set of coupled Boltzmann equations in Eq. (B1) needs to be considered. Nevertheless, even in this case several approximations are possible for our model, as we explain below.

First of all, the coannihilation of different φ_i components into SM particles, $\varphi_i \varphi_j \rightarrow XX$ ($i \neq j$), can be safely neglected in our model. In benchmarks that survive the experimental constraints the off-diagonal couplings of the lightest FGB to φ are much smaller than the

diagonal ones, see Fig. 16. Secondly, in the calculation of DM relic density we also neglect the flavor-changing DM scattering off the thermal background, $\varphi_i X \rightarrow \varphi_j X$. The $\varphi_i X \rightarrow \varphi_j X$ scattering can be important if $\langle \sigma(\varphi_i X \rightarrow \varphi_j X) v_{\text{lab}} \rangle / \langle \sigma(\varphi_i \varphi_j \rightarrow X X) v_{\text{lab}} \rangle \gtrsim n_{\varphi_j} / n_X^{\text{EQ}} \sim 10^{-9}$. In this case the off-diagonal couplings of $\mathcal{O}(10^{-4})$ relative to the diagonal ones are in principle large enough to have $\mathcal{O}(1)$ effects on the relic density, and neglecting $\varphi_i X \rightarrow \varphi_j X$ may not be justified. Therefore, for the benchmarks with $(\hat{g}_X^{24})_{23}/(\hat{g}_X^{24})_{33} > 3 \times 10^{-4}$ and small mass splittings among φ , we explicitly verified using **MadDM** that neglecting $\varphi_i X \rightarrow \varphi_j X$ scattering leads to a change in DM relic density smaller than $\mathcal{O}(30\%)$.

Finally, we are able to neglect the pure DM scattering process in the third line of Eq. (B1) since $\langle \sigma(\varphi_i \varphi_j \leftrightarrow \varphi_k \varphi_\ell) v_{\text{lab}} \rangle \ll \langle \sigma(\varphi_i \varphi_j \leftrightarrow X X) v_{\text{lab}} \rangle$ in our model. The largest contribution to this process is from diagonal couplings between the FGB and DM. This process can couple the evolution of the DM species if $\langle \sigma(\varphi_i \varphi_j \leftrightarrow \varphi_k \varphi_\ell) v_{\text{lab}} \rangle \sim \langle \sigma(\varphi_i \varphi_j \leftrightarrow X X) v_{\text{lab}} \rangle$. The diagonal FGB couplings to the quarks and to the DM of the same generation are approximately equal. By accounting for the color factors and the multiplicity of channels when annihilating into SM fields one concludes that the pure DM scattering is indeed subleading.

Therefore, for almost mass degenerate φ_i it is sufficient to consider a set of uncoupled Boltzmann equations

$$\frac{dn_{\varphi_i}}{dt} + 3Hn_{\varphi_i} = - \sum_j \langle \sigma(\varphi_i \varphi_j \leftrightarrow X X) v_{\text{lab}} \rangle (n_{\varphi_i}^2 - n_{\varphi_i}^{\text{EQ}2}). \quad (\text{B2})$$

The DM relic abundance is in this case the sum of relic abundances for each of the three components obtained from the above set of equations (the heavy φ components, in our case φ_2 and φ_3 , decay after their respective freeze-outs and contribute to the φ_1 DM relic abundance). In contrast, for large mass splittings the heavy φ components are irrelevant for the calculation of the DM relic abundance. This is then obtained from Eq. (B2) by considering only the lightest DM state, in our case φ_1 .

We calculate the DM relic abundance from Eq. (B2) using the freeze-out approximation [26], which gives

$$\Omega h^2 = \frac{1.07 \times 10^9 \text{ GeV}^{-1}}{J(x_f) \sqrt{g_*} M_{Pl}}, \quad (\text{B3})$$

where $M_{Pl} = 1.22 \times 10^{19} \text{ GeV}$, g_* is the total number of effectively relativistic degrees of freedom at the time of the freeze-out, and

$$J(x_f) = \int_{x_f}^{\infty} dx \frac{\langle \sigma v_{\text{lab}} \rangle_{\text{th}}}{x^2}. \quad (\text{B4})$$

The freeze-out temperature ($x_f = m_{\varphi_1}/T_f$) is obtained by solving

$$x_f = \ln \frac{0.038 g_{\text{eff}} M_{Pl} m_{\varphi_1} \langle \sigma v_{\text{lab}} \rangle_{\text{th}}}{\sqrt{g_*} x_f}, \quad (\text{B5})$$

where the thermally-averaged cross section is

$$\langle \sigma v_{\text{lab}} \rangle_{\text{th}} = \frac{2x^{\frac{3}{2}}}{\sqrt{\pi}} \int_0^\infty \sigma_{\text{eff}} v_{\text{lab}} \sqrt{\epsilon} e^{-x\epsilon} d\epsilon, \quad (\text{B6})$$

with $v_{\text{lab}} = 2\sqrt{\epsilon(1+\epsilon)}/(1+2\epsilon)$ and $\epsilon = s/(2m_{\varphi_1})^2 - 1$. The freeze-out approximation is accurate to a few percent with respect to the full numerical solution of the Boltzmann equation [25].

The fermionic flavored DM annihilates through the s-channel exchange of FGBs. In this case, the integration over x can be performed analytically and the double integral in Eq. (B4) reduces to a single one that can be efficiently evaluated numerically. In particular,

$$J(x_f) = \int_0^\infty 2\sigma v_{\text{lab}} \text{Erfc}(\sqrt{x_f \epsilon}) d\epsilon. \quad (\text{B7})$$

We evaluate the above integral numerically in the parameter scan.

In the annihilation cross section of the fermionic flavored DM we keep the dominant contribution – the s -channel exchange of the lightest FGB, A^{24} . The annihilation cross section for $\chi_i \bar{\chi}_i \rightarrow \bar{u}_j u_j$ (and similarly for $\chi_i \bar{\chi}_i \rightarrow \bar{d}_j d_j$) is given by

$$\begin{aligned} \sigma(\chi_i \bar{\chi}_i \rightarrow \bar{u}_j u_j) = & \frac{(\hat{g}_\chi^{24})_{ii}^2}{4\pi} \sqrt{\frac{s - 4m_{u_j}^2}{s - 4m_{\chi_i}^2}} \left(1 + \frac{2m_{\chi_i}^2}{s}\right) \times \\ & \times \frac{(\hat{\mathcal{G}}_V^u)_{jj,24}^2 (s + 2m_{u_j}^2) + (\hat{\mathcal{G}}_A^u)_{jj,24}^2 (s - 4m_{u_j}^2)}{(s - m_{A^{24}}^2)^2 + m_{A^{24}}^2 \Gamma_{A^{24}}^2}, \end{aligned} \quad (\text{B8})$$

where the vector and axial-vector couplings to quarks, $\hat{\mathcal{G}}_{A,V}$, were defined in Eq. (25), \sqrt{s} is the center-of-mass energy and $\Gamma_{A^{24}}$ is the total decay width of the lightest FGB. The decay rate for $A^{24} \rightarrow \bar{u}_j u_j$ assuming $m_{A^{24}} > 2m_{u_j}$ is

$$\Gamma(A^{24} \rightarrow \bar{u}_j u_j) = \frac{m_A^{24}}{4\pi} \sqrt{1 - \frac{4m_{u_j}^2}{m_{A^{24}}^2}} \left[(\hat{\mathcal{G}}_V^u)_{jj,24}^2 \left(1 + \frac{2m_{u_j}^2}{m_{A^{24}}^2}\right) + (\hat{\mathcal{G}}_A^u)_{jj,24}^2 \left(1 - \frac{4m_{u_j}^2}{m_{A^{24}}^2}\right) \right]. \quad (\text{B9})$$

The rate for $A^{24} \rightarrow \chi_i \bar{\chi}_i, \bar{d}_j d_j$ is obtained after trivial replacements for masses and couplings (and dividing by the N_c color factor for decays to $\chi_i \bar{\chi}_i$). The total FGB decay rate is obtained after summing over all kinematically allowed decay channels.

Appendix C: Higgs coupling Feynman rules

As noted in Sec. [IV E](#), the $h\bar{f}f$ Feynman rules given in Appendix A.1 of Ref. [\[23\]](#) contain a typo. The corrected Feynman rules are given here.

$$\begin{array}{c} \bar{f} \\ \nearrow \\ h \text{ ---} \\ \searrow \\ f \end{array} = \frac{i}{\sqrt{2}} (C_L P_L + C_R P_R) \quad (\text{C1})$$

where the couplings C_L and C_R are:

$$\begin{aligned}
h\bar{u}_i u_i &: C_L = C_R = +\lambda_u s_{uRi} c_{uLi} \\
h\bar{u}'_i u'_i &: C_L = C_R = -\lambda_u c_{uRi} s_{uLi} \\
h\bar{u}_i u'_i &: \begin{cases} C_R = -\lambda_u c_{uRi} c_{uLi} \\ C_L = +\lambda_u s_{uRi} s_{uLi} \end{cases} \\
h\bar{u}'_i u_i &: \begin{cases} C_R = +\lambda_u s_{uRi} s_{uLi} \\ C_L = -\lambda_u c_{uRi} c_{uLi} \end{cases}
\end{aligned} \tag{C2}$$

- [1] G. Jungman, M. Kamionkowski, and K. Griest, Phys.Rept. **267**, 195 (1996), hep-ph/9506380.
- [2] M. Hirsch, S. Morisi, E. Peinado, and J. Valle, Phys.Rev. **D82**, 116003 (2010), 1007.0871.
- [3] M. Boucenna, M. Hirsch, S. Morisi, E. Peinado, M. Taoso, et al., JHEP **1105**, 037 (2011), 1101.2874.
- [4] D. Meloni, S. Morisi, and E. Peinado, Phys.Lett. **B697**, 339 (2011), 1011.1371.
- [5] M. Lindner, D. Schmidt, and T. Schwetz, Phys.Lett. **B705**, 324 (2011), 1105.4626.
- [6] B. Batell, J. Pradler, and M. Spannowsky, JHEP **1108**, 038 (2011), 1105.1781.
- [7] B. Batell, T. Lin, and L.-T. Wang, JHEP **1401**, 075 (2014), 1309.4462.
- [8] L. Lopez-Honorez and L. Merlo, Phys.Lett. **B722**, 135 (2013), 1303.1087.
- [9] B. Grinstein, M. Redi, and G. Villadoro, JHEP **1011**, 067 (2010), 1009.2049.
- [10] P. Agrawal, B. Batell, D. Hooper, and T. Lin, Phys.Rev. **D90**, 063512 (2014), 1404.1373.
- [11] C.-J. Lee and J. Tandean (2014), 1410.6803.
- [12] F. Bishara and J. Zupan (2014), 1408.3852.
- [13] P. Agrawal, M. Blanke, and K. Gemmler, JHEP **1410**, 72 (2014), 1405.6709.

- [14] P. Agrawal, S. Blanchet, Z. Chacko, and C. Kilic, Phys.Rev. **D86**, 055002 (2012), 1109.3516.
- [15] A. Hamze, C. Kilic, J. Koeller, C. Trendafilova, and J.-H. Yu (2014), 1410.3030.
- [16] A. Kumar and S. Tulin, Phys.Rev. **D87**, 095006 (2013), 1303.0332.
- [17] J. F. Kamenik and J. Zupan, Phys.Rev. **D84**, 111502 (2011), 1107.0623.
- [18] J. Kile, A. Kobach, and A. Soni (2014), 1411.1407.
- [19] J. Kile and A. Soni, Phys.Rev. **D84**, 035016 (2011), 1104.5239.
- [20] L. Calibbi, A. Crivellin, and B. Zaldivar (2015), 1501.07268.
- [21] G. D’Ambrosio, G. Giudice, G. Isidori, and A. Strumia, Nucl.Phys. **B645**, 155 (2002), hep-ph/0207036.
- [22] C. Smith, Phys.Rev. **D85**, 036005 (2012), 1105.1723.
- [23] A. J. Buras, M. V. Carlucci, L. Merlo, and E. Stamou, JHEP **1203**, 088 (2012), 1112.4477.
- [24] A. L. Kagan, G. Perez, T. Volansky, and J. Zupan, Phys.Rev. **D80**, 076002 (2009), 0903.1794.
- [25] P. Gondolo and G. Gelmini, Nucl.Phys. **B360**, 145 (1991).
- [26] K. Griest and D. Seckel, Phys.Rev. **D43**, 3191 (1991).
- [27] M. Backovic, K. Kong, and M. McCaskey, Physics of the Dark Universe **5-6**, 18 (2014), 1308.4955.
- [28] A. Alloul, N. D. Christensen, C. Degrande, C. Duhr, and B. Fuks, Comput.Phys.Commun. **185**, 2250 (2014), 1310.1921.
- [29] B. Fields and S. Sarkar (2006), astro-ph/0601514.
- [30] W. Hu and J. Silk, Phys.Rev. **D48**, 485 (1993).
- [31] W. Hu and J. Silk, Phys.Rev.Lett. **70**, 2661 (1993).
- [32] R. Essig, E. Kuflik, S. D. McDermott, T. Volansky, and K. M. Zurek, JHEP **1311**, 193 (2013), 1309.4091.
- [33] F. Iocco, G. Mangano, G. Miele, O. Pisanti, and P. D. Serpico, Phys.Rept. **472**, 1 (2009), 0809.0631.
- [34] D. Lindley, Astrophys.J. **294**, 1 (1985).
- [35] M. Reno and D. Seckel, Phys.Rev. **D37**, 3441 (1988).
- [36] S. Dimopoulos, R. Esmailzadeh, L. J. Hall, and G. Starkman, Astrophys.J. **330**, 545 (1988).
- [37] R. J. Scherrer and M. S. Turner, Astrophys.J. **331**, 19 (1988).
- [38] J. R. Ellis, G. Gelmini, J. L. Lopez, D. V. Nanopoulos, and S. Sarkar, Nucl.Phys. **B373**, 399 (1992).

- [39] M. Kawasaki, K. Kohri, and T. Moroi, Phys.Rev. **D71**, 083502 (2005), astro-ph/0408426.
- [40] G. Belanger, F. Boudjema, A. Pukhov, and A. Semenov, Comput.Phys.Commun. **180**, 747 (2009), 0803.2360.
- [41] G. Arcadi, Y. Mambrini, M. H. G. Tytgat, and B. Zaldivar, JHEP **1403**, 134 (2014), 1401.0221.
- [42] D. Akerib et al. (LUX Collaboration), Phys.Rev.Lett. **112**, 091303 (2014), 1310.8214.
- [43] A. Urbano and W. Xue (2014), 1412.3798.
- [44] J. M. Cline and K. Kainulainen, JCAP **1301**, 012 (2013), 1210.4196.
- [45] P. Junnarkar and A. Walker-Loud, Phys.Rev. **D87**, 114510 (2013), 1301.1114.
- [46] J. Alarcon, J. Martin Camalich, and J. Oller, Phys.Rev. **D85**, 051503 (2012), 1110.3797.
- [47] L. Alvarez-Ruso, T. Ledwig, J. Martin Camalich, and M. Vicente Vacas, EPJ Web Conf. **73**, 04015 (2014).
- [48] A. Crivellin, F. D’Eramo, and M. Procura, Phys.Rev.Lett. **112**, 191304 (2014), 1402.1173.
- [49] A. Crivellin, M. Hoferichter, and M. Procura, Phys.Rev. **D89**, 054021 (2014), 1312.4951.
- [50] M. Boudaud, M. Cirelli, G. Giesen, and P. Salati (2014), 1412.5696.
- [51] O. Adriani, G. Bazilevskaya, G. Barbarino, R. Bellotti, M. Boezio, et al., JETP Lett. **96**, 621 (2013).
- [52] M. Ackermann et al. (Fermi-LAT) (2015), 1503.02641.
- [53] M. R. Buckley, E. Charles, J. M. Gaskins, A. M. Brooks, A. Drlica-Wagner, et al., Phys.Rev.D (2015), 1502.01020.
- [54] M. Ackermann et al. (Fermi LAT Collaboration) (2015), 1501.05464.
- [55] G. Aad et al. (ATLAS Collaboration) (2014), 1407.1376.
- [56] S. Chatrchyan et al. (CMS Collaboration), Phys.Lett. **B729**, 149 (2014), 1311.7667.
- [57] E. Eichten, I. Hinchliffe, K. D. Lane, and C. Quigg, Rev.Mod.Phys. **56**, 579 (1984).
- [58] K. D. Lane and M. Ramana, Phys.Rev. **D44**, 2678 (1991).
- [59] A. J. Buras, S. Jager, and J. Urban, Nucl.Phys. **B605**, 600 (2001), hep-ph/0102316.
- [60] J. Laiho, E. Lunghi, and R. S. Van de Water, Phys.Rev. **D81**, 034503 (2010), 0910.2928, URL <http://www.latticeaverages.org>.
- [61] A. J. Buras, D. Guadagnoli, and G. Isidori, Phys.Lett. **B688**, 309 (2010), 1002.3612.
- [62] A. J. Buras and D. Guadagnoli, Phys.Rev. **D78**, 033005 (2008), 0805.3887.
- [63] J. Brod and M. Gorbahn, Phys.Rev.Lett. **108**, 121801 (2012), 1108.2036.

- [64] J. Brod and M. Gorbahn, Phys.Rev. **D82**, 094026 (2010), 1007.0684.
- [65] A. J. Buras, L. Merlo, and E. Stamou, JHEP **1108**, 124 (2011), 1105.5146.
- [66] M. Misiak, H. Asatrian, K. Bieri, M. Czakon, A. Czarnecki, et al., Phys.Rev.Lett. **98**, 022002 (2007), hep-ph/0609232.
- [67] P. Gambino and M. Misiak, Nucl.Phys. **B611**, 338 (2001), hep-ph/0104034.
- [68] M. Misiak and M. Steinhauser, Nucl.Phys. **B764**, 62 (2007), hep-ph/0609241.
- [69] M. Bona et al. (UTfit), JHEP **0803**, 049 (2008), 0707.0636.
- [70] C. Degrande, C. Duhr, B. Fuks, D. Grellscheid, O. Mattelaer, et al., Comput.Phys.Commun. **183**, 1201 (2012), 1108.2040.
- [71] R. S. Chivukula and H. Georgi, Phys. Lett. B **188**, 99 (1987).
- [72] E. Gabrielli and G. F. Giudice, Nucl. Phys. B **433**, 3 (1995) [Nucl. Phys. B **507**, 549 (1997)] [[hep-lat/9407029](#)].
- [73] A. Ali and D. London, Eur. Phys. J. C **9**, 687 (1999) [[hep-ph/9903535](#)].
- [74] A. J. Buras, P. Gambino, M. Gorbahn, S. Jager and L. Silvestrini, Phys. Lett. B **500**, 161 (2001) [[hep-ph/0007085](#)].
- [75] A. J. Buras, Acta Phys. Polon. B **34**, 5615 (2003) [[hep-ph/0310208](#)].